Chapter 3

Synthesis, Characterization and application of uriede based thiazole derivatives

3.1 Introduction

The term 'Gels' was first coined in 1861 by Thomas Graham, and since then various definitions have been put forward till now[1]. Gels are the system where a liquid phase is immobilized by the solid phase and rheologically behaves like the solid, despite having a larger proportion of liquid[2]. Low Molecular Mass Organic Gelators (LMOGs) are the key component forming a three-dimensional network capable of immobilizing solvent through surface tension and capillary forces. LMOGs are commonly comprised of hydrogen bond-forming groups such as urea [3], amide[4,5] and organic backbone consisting of sugar[6], nucleotides[7], and cholesterol[8] moiety, which forms the macroscopic fibrillar networks.

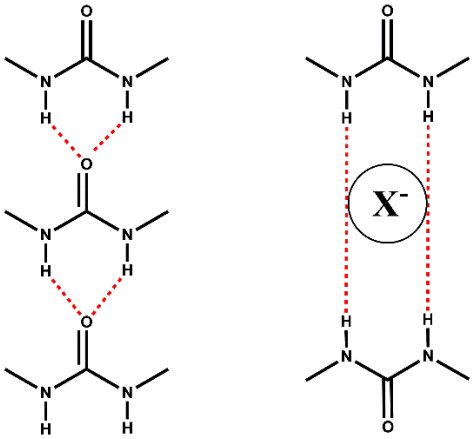

Scheme 3.1 *Hydrogen bonding in urea motif(left)and Interaction of urea with halide(right)*

Despite the exponential growth of the new gelator and its application, designing of new gelator with a predictable application is a daunting task. One of the major strategies for designing new LMOGs is the incorporation of hydrogen bonding sites capable of forming a 1-D hydrogen bonding network[9]. Undoubtedly, the choice of such functional groups is urea and amide due to their robust 1D supramolecular synthons. Our recent success with the design, synthesis, and applications of new LMOGs containing thiazole[4] and pivalic acid[10] as backbone and amide functional groups, prompted us to explore urea as a 1-D H-bond structure directing element. Moreover, the presence of urea moiety in a molecule endowed them with potential applications in the field of cosmetics[11], anion recognition[12] and biological activities[13–15].The 1D hydrogen-bonded supramolecular synthons of urea moiety and their probable interaction with halide ions are shown in scheme 3.1[12]. Even though thiazole-urea-containing compounds are well known for their antioxidant[16],

herbicidal[17], and anticancer[18] activities, but have never been explored as potential LMOGs.

In the present study, we synthesized a series of compounds having thiazole moiety, hydrogen bonding site (urea functional group), and long alkyl chain (UTz **1–7**). The systematic increase in the aliphatic long chain from decyl to heptadecyl [(CH_2) or methylene functional group of aliphatic chain varying from 10 to 17, except hexadecyl n = 13] was carried out to explore the role of van der Waals interaction (or hydrophobic effect) on gelation process along with reliable 1D hydrogen bonding urea functional group. (See Scheme 3.2).

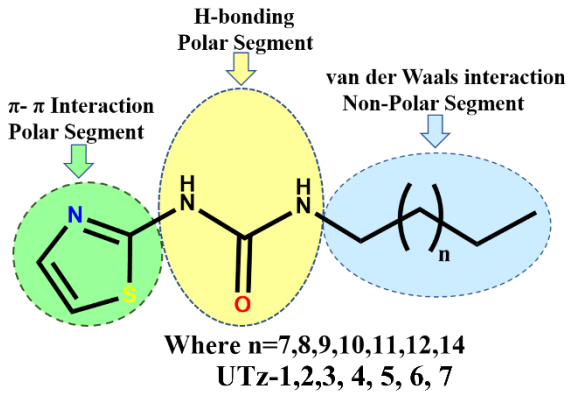

No of methylene group	Name of compound
10	UTz-1
11	UTz-2
12	UTz-3
13	UTz-4
14	UTz-5
15	UTz-6
17	UTz-7

Scheme 3.2 *List of organic compounds synthesized (UTz **1–7**)*

All the synthesized compounds were investigated for their potential gelation behaviour towards polar/non-polar solvents and the mixture of solvents. Even though none of the synthesized compounds turned out to be hydrogelator but all were found to be capable of gelling a mixture of solvents containing water. Moreover, the anion sensing capability of these compounds showed strong selectivity towards iodide ions. Iodide ion sensing is active research mainly due to its influence on human health[19]. However, a simple and efficient method of iodide ion sensing is highly desirable as the current methods such as Raman scattering[20], electrochemical method[21], and mass spectrometry[22], require long sample preparation and sophisticated instrumentation facility.

3.2 Materials and Physical measurements

3.2.1 Materials

Long chain aliphatic carboxylic acids and 2-aminothiazole were purchased from Sigma Aldrich. Diphenylphosphorylazide and triethylamine were obtained from CDH

(P) Ltd., India and used without any further purification. Solvents for gelation studies were reagent grade and used without any distillation, Further solvents for synthesis was purified and dried over molecular sieve.

3.2.2 Rheological studies

The rheology studies of the organogels (at MGC value) were recorded using TA Instruments ARES G2 Rheometer. Amplitude sweep was performed at room temperature (23˚C) using 50 mm parallel plates maintained at a gap of 1 mm with a frequency variation of 10 rad/sec.

3.2.3 NMR Spectroscopy

NMR spectra of Compound was recorded in $CDCl_3$ on BRUKER ADVANCE, 400MHz Spectrometer at 298 kelvin temperature.

3.2.4 FT-IR Spectroscopy

FT-IR Studies of UTz **1-7** and its xerogel were performed in solid-state using KBr pellet on BRUKER ALPHA FT-IR Spectrometer and spectra were recorded in the wavenumber range from 400-4000 cm^{-1}.

3.2.5 Polarized Optical Microscopy

Supersaturated gelator solution was placed on glass slide and allowed to cool down at room temperature to form gel and this gel was directly observed and images were taken using Leica DM 2500P Polarising optical microscope provided with the Linkam heating stage.

3.2.6 SEM Measurements

Hot solution of gelator in respective solvents was placed on sample holder and allowed to cool to form gel, and then dried under vacuum. Dried gel was subjected to gold sputtering using POLARON SC7620 Sputter Coater and this gold coated dried gel was subjected to JEOL JSM 5610 LV SEM instrument after carbon coating.

3.2.7 Powder X-ray Diffraction

Powder XRD pattern of the neat gelator (Bulk) and xerogel (obtain from slow evaporation) was obtained from X'pert Pan Analytical Powder diffractometer with Cu KR (1.54 Å) radiation (45 kV, 40 mA). The proportional counter detector collected over the range of 2θ=10-50°.

3.2.8 UV-Visible Spectroscopy studies

The electronic spectra (in THF at room temperature) in the range of 200-600 nm were recorded on a model JASCO 7600 UV-VIS spectrophotometer.

3.2.9 Fluorescence study

Fluorescence spectra were recorded on a JASCO FP-6300 fluorescence spectrophotometer.

3.2.10 SANS Studies

Small-angle neutron scattering experiments were performed on the SANS diffractometer at Guide Tube Laboratory, Dhruva Reactor, Bhabha Atomic Research Centre, Mumbai, India [23]. In SANS, one measures the coherent differential scattering cross-section ($d\Sigma/d\Omega$) per unit volume as a function of wave vector transfer Q ($=4\pi \sin\theta/\lambda$, where k is the wavelength of the incident neutrons and 2θ is the scattering angle). The mean wavelength of the monochromatized beam from the neutron velocity selector is 5.2 Å with a spread of $\Delta\lambda/\lambda \sim 15\%$. The angular distribution of neutrons scattered by the sample is recorded using a 1 m long one-dimensional He^3 position-sensitive detector. The instrument covers a Q-range of 0.015–0.26 $Å^{-1}$.

The data have been analyzed by comparing the scattering from different models to the experimental data.

3.3 Experimental Procedures

3.3.1 Gelation Studies

Gelation studies of the synthesized compound were carried out by taking a weighted amount (10 mg) of the powdered compound in the known amount of solvent (0.5 mL), and the system is heated until the dissolution of the powder in the oil/water bath. The resultant solution was kept for half an hour to cool down at 25 ˚C and the immobilization of the solvent was tested by inverting the vial upside down. The free-flowing clear system is considered as ‘‘S” (soluble), the compound which is soluble on heating, but crystallizes and precipitates on cooling is termed as ‘‘C” (crystallization) and ‘‘P” (precipitation) and immobilization of solvent (Observed when the vial was inverted) is denoted as ‘‘G”. The MGC (Minimum Gelator Concentration) for each gel/solvent system is determined by a gradual increase in the solvent by 0.5 mL till the gelation is observed. The weighted amount of solvent/compounds are used for the determination of solvent gelled by the

compounds. The gel strength or sol–gel transition temperature (T_{gel}) was determined by gradual heating (0.5˚C per minute) of the vial containing gel (at MGC value in 1 mL solvent) using 'ball-drop-method' and 'inverted vial method'. Each experiment is repeated at least 3 times to get the average T_{gel} value for a given solvent/gelator system.

3.3.2 UV-visible titration studies

The stock solution of UTz-**1**(6 **μ**M) was prepared and the stock solution of various anions (100 **μ**M) (Tetrabutylammonium salts of Fluoride, bromide and dihydrogenphosphate) were prepared in Tetrahydrofuran (THF). The calculated amount of stock solution of anion was added to the 2.5 mL of **UTz-1** solution to get the required concentration of anion to carry out scan.

3.3.3 Fluorescence titration

The stock solution of UTz-**1**(6 **μ**M) was prepared and the stock solution Tetrabutylammonium fluoride (TBAF) (100 **μ**M) was prepared in tetrahydrofuran (THF). The calculated amount of stock solution of TBAF was added to the 2.5 mL of **UTz-1** solution to get the required concentration of TBAF to carry out spectroscopic scans.

3.3.4 Determination of stoichiometry

Continuous variation method was used to determine the stoichiometry of the host guest complex. In this method solutions of equal concentration of host and guest are made in the appropriate solvent. After that, solution of host and guest mixed with the different proportion maintaining the total volume fixed around 3.0 mL. The compositions are 3:0, 2.8:0.2, 2.5:0.5, 2.2:0.8, 2:1, 1.8:1.2, 1.5:1.5, 1:2, 0.8:2.2, 0.5:2.5, and 0.2:2.8 respectively. These solutions are kept for one hour at room temperature with the occasional stirring. The emission spectra of these solution are taken.

3.3.5 SANS Analysis

The SANS data for gels were analysed employing the traditional two-stage network model of the polymer gels[24–26] comprising two terms described as

$$I(Q) = \frac{I(0)}{1+Q^2\xi^2} + \frac{A}{Q^n} + Bkg \qquad (1)$$

where, the first term is a Lorentzian function, called as Ornstein–Zernike equation which describes the scattering caused by the compositional fluctuations, and its Fourier transform gives the correlations. I(0) denotes the forward scattering and ξ is the correlation length (is often described as a blob where the excluded volume effects are observed) of the system.

Since there is no low-*Q* cut-off is observed in the SANS data, it implies that the size of these inhomogeneities is larger than that can be seen in the limited *Q*-range of the instrument. It has been incorporated in the second term which is a power law (depicting the mass fractal dimension) accounting for the large moieties present in the sample.

For mass fractals, the mass $M(r)$ inside a spherical surface with radius r inscribing the structure is given by $M(r)\ \alpha\ r^d$, $d \leq 3$ and $S(Q)$ for such fractal structure can be expressed as [27,28]

$$S_{mf}(Q) = 1 + \frac{1}{(QR_b)^{D_m}} \frac{D_m \Gamma(D_m - 1)}{[1 + (Q\xi)^{-2}]^{[(D_m-1)/2]}} \times \sin[(D_m - 1)\tan^{-1}(Q\xi)] \qquad (2)$$

where $\Gamma(x)$ is the gamma function of argument x. R_b is the building-block size forming the fractal structure. D_m and ξ are the fractal dimension and the correlation length of the fractal network, respectively.

It may be mentioned that the scattering intensity from mass fractal structures is governed by power-law behaviour in a definite Q range, scattering intensity shows linearity [$I(Q) \sim Q^{-\alpha}$] in profile in the intermediate Q values ($1/\xi < Q < 1/R_b$).

$$\frac{d\Sigma}{d\Omega}(Q) \sim Q^{-D_m} \qquad \frac{1}{\xi} < Q < \frac{1}{R_b} \text{ for mass fractals} \qquad (3)$$

The value of exponent α varies between 1 and 3 for mass fractals.

3.3.6 Synthesis

Acid (1 eq. wt., 1 g), triethylamine (2.2 eq. wt.), and diphenylphosphorylazide (1.2 eq. wt.) was dissolved in dry toluene. The solution was refluxed over 3 hours. The solution was kept at 0 ˚C and the suspension of 2-aminothiazole is added dropwise and stirred for 15 Hours at Room temperature (25 ˚C) and monitored by TLC until completion (Scheme 3.3). The reaction mixture, obtained after completion, was washed with water and saturated $NaHCO_3$ and then with dil. HCl. and dried over Na_2SO_4. Finally, compounds were recrystallized from ethyl acetate.

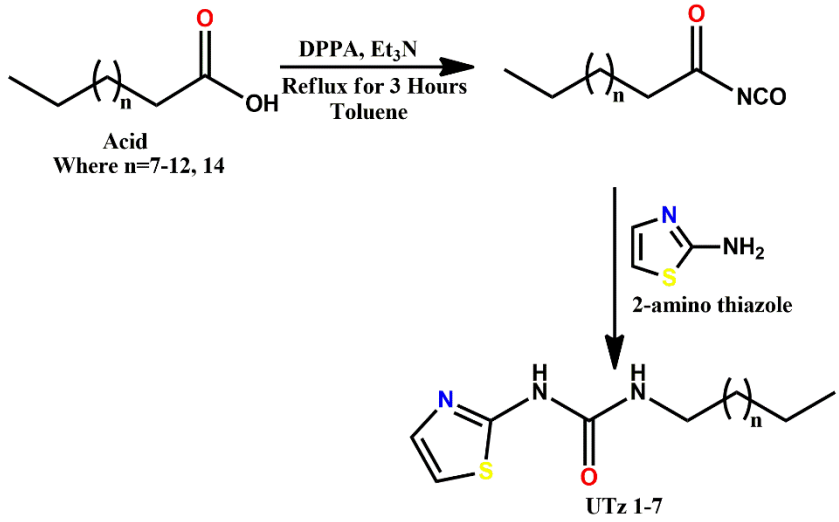

Scheme 3.3 Synthetic scheme for UTz 1-7

Analytical Data

UTz-1(1-decyl-3-(thiazol-2-yl)urea): (0.614 g, Yield 40.4 %) m.p. 107°C ^{1}H NMR (400 MHz, CDCl3, TMS): 11.347 (s, 1H, NH), 7.448 (d, 1H; CH), 7.004 (d, 1H; CH), 2.560 -2.522 (t, 2H; CH_2), 1.820–1.269(m, 16H, CH_2),0.899-0.874 (t, 3H; CH_3). MS (EI): m/z 283.172 $[M]^+$. FTIR (KBr): 3369, 3247, 3178, 2919, 2852, 1686, 1650, 1574, 1533, 1469, 1446, 1375, 1320, 1278, 1236, 1163, 1146, 1065, 920, 868, 773, 718, 697, 625, 520 cm^{-1}

UTz-2(1-undecyl-3-(thiazol-2-yl)urea): (0.742 g, 50.1%) m.p. 100°C ^{1}H NMR (400 MHz, DMSO, TMS): 10.296 (s, 1H, NH), 7.277 (d, 1H; CH), 6.999 (d, 1H; CH), 6.536 (s, 1H, NH), 3.118-3.070 (q, 2H; CH_2), 1.412–1.227(m, 18H, CH_2),0.854-0.820 (t, 3H; CH_3). MS (EI): m/z 297.187 $[M]^+$. FTIR (KBr): 3369, 3248, 3188, 3089, 2954, 2918, 2851, 1686, 1650, 1575, 1533, 1470, 1446, 1375, 1320, 1297, 1163, 1065, 960, 899, 790, 769, 717, 697, 625, 560, 512 cm^{-1}.

UTz-3(1-(1-dodecyl-3-(thiazol-2-yl)urea): (0.61 g, 45.5%) m.p. 111 °C ^{1}H NMR (400 MHz, DMSO, TMS): 10.310 (s, 1H, NH), 7.283 (d, 1H; CH), 6.990 (d, 1H; CH), 6.532 (s, 1H, NH), 3.124-3.075 (q, 2H; CH_2), 1.432–1.231(m, 20H, CH_2),0.859-0.829 (t, 3H; CH_3). MS (EI): m/z 311.203 $[M]^+$. FTIR (KBr): 3178, 2919, 2852, 1687, 1586, 1467, 1381, 1326, 1282, 1173,1067, 960, 874, 809, 778, 719, 625, 520 cm^{-1}

UTz-4(1-tridecyl-3-(thiazol-2-yl)urea): (0.68 g, 48.2%) m.p. 107 °C ^{1}H NMR (400 MHz, DMSO, TMS): 10.303 (s, 1H, NH), 7.288 (d, 1H; CH), 7.000 (d, 1H; CH), 6.516 (s, 1H, NH), 3.125-3.075 (q, 2H; CH2), 1.418–1.233(m, 22H, CH_2),0.866-0.831 (t, 3H; CH_3). MS (EI): m/z 325.219 $[M]^+$. FTIR (KBr): 3369, 3248, 3188, 3089, 2953, 2917, 2850, 1686, 1650 1575, 1535, 1470, 1446, 1375, 1320, 1299, 1278, 1240, 1163, 1146, 1064, 916, 868, 809, 770, 717, 610, 561 cm^{-1}

UTz-5(1-tetradecyl-3-(thiazol-2-yl)urea): (0.59 g, 42.8%) m.p. 111 °C ^{1}H NMR (400 MHz, DMSO, TMS): 10.302 (s, 1H, NH), 7.287 (d, 1H; CH), 7.000 (d, 1H; CH),

6.505 (s, 1H, NH), 3.124-3.075 (q, 2H; CH2), 1.433-1.404(t, 2H; CH_2), 1.233(m, 22H, CH_2),0.866- 0.831 (t, 3H; CH_3). MS (EI): m/z 339.219 $[M]^+$. FTIR (KBr): 3369, 3248, 3188, 3089, 2953, 2917, 2850, 1686, 1650, 1675, 1575, 1535, 1471, 1446 1376, 1320, 1279, 1239, 1164, 1146, 1065, 924, 869, 768, 717, 696, 610, 561 cm^{-1}.

UTz-6(1-pentadecyl-3-(thiazol-2-yl)urea): (0.61 g, 45.1%) m.p. 115 °C ^{1}H NMR (400 MHz, DMSO, TMS): 10.302 (s, 1H, NH), 7.287 (d, 1H; CH), 7.000 (d, 1H; CH), 6.505 (s, 1H, NH), 3.124-3.075 (q, 2H; CH2), 1.433-1.404(t, 2H; CH_2), 1.233(m, 24H, CH_2),0.866- 0.831 (t, 3H; CH_3). MS (EI): m/z 353.219 $[M]^+$. FTIR (KBr): 3369, 3248, 3188, 3089, 2953, 2917, 2850, 1686, 1650, 1675, 1575, 1535, 1471, 1446 1376, 1320, 1279, 1239, 1164, 1146, 1065, 924, 869, 768, 717, 696, 610, 561 cm^{-1}.

UTz-7(1-heptadecyl-3-(thiazol-2-yl) urea): (0.64 g, 48.5%) m.p. 115 °C ^{1}H NMR (400 MHz, DMSO, TMS): 10.617 (s, 1H, NH), 7.271 (d, 1H; CH), 6.975 (d, 1H; CH), 6.915 (s, 1H, NH), 3.114-3.065 (q, 2H; CH_2), 1.413–1.228(m, 28H, CH_2),0.863-0.829 (t, 3H; CH_3). MS (EI): m/z 367.26 $[M]^+$. FTIR (KBr): 3369, 3250, 2917, 2850, 1686, 1650, 1576, 1535, 1471, 1446, 1376, 1321, 1279, 1246, 1163,1065, 869, 770, 717, 696, 610 cm^{-1}.

For NMR and IR spectra refer to supporting information.

3.4 RESULTS AND DISCUSSION

3.4.1 Gelation studies

A set of 18 solvents including water with various polarities was selected for gelation studies of UTz **1–7**. Additionally, seven mixtures of solvents with water (1:1 volume/volume) were also explored as a gelling solvent to see the effect of polarity on the gelling ability of synthesized compounds and summarized in Table 3.1.

Table 3.1 *Gelation profile of UTz 1-7*

Solvents	UTz 1	UTz 2	UTz 3	UTz 4	UTz 5	UTz 6	UTz 7
CCl_4	P	P	P	P	P	P	P
n-Hexane	P	I	P	I	P	P	P
Cyclohexane	P	P	P	P	P	P	P
Toluene	S	S	S	S	S	S	S
Chlorobenzene	C	C	C	C	C	C	C
Isopropanol	P	P	P	P	P	P	P
Tetrahydrofuran	S	S	S	S	S	S	S
Methanol	S	P	P	P	P	P	P
Ethanol	P	P	P	P	P	P	P
Acetone	P	P	P	P	P	P	P
Acetonitrile	P	**G(4.40)**	**G(4.25)**	**G(8.60)**	**G(3.60)**	**G(4.45)**	P
3˚-Butanol	P	S	S	S	S	P	S
n-Butanol	P	S	S	S	S	S	S
n-Pentanol	S	S	S	S	S	S	S
n-Decanol	S	S	S	S	S	S	S
Propan-1,2-diol	**G(4.13)**	**G(1.98)**	**G(2.40)**	**G(2.10)**	**G(1.70)**	**G(5.42)**	**G(5.50)**
Dimethylsulphoxide	S	S	S	S	S	S	S
Dimethylformamide	S	S	S	S	S	S	S
Water	P	P	P	P	P	P	P
Methanol:Water(1:1)	P	P	P	P	P	P	P
Ethanol:Water(1:1)	**G(1.57)**	**G(2.8)**	**G(1.51)**	**G(1.61)**	**G(3.50)**	**P**	**G(5.50)**
THF:Water(1:1)	P	P	P	P	P	P	P
DMSO:Water(1:1)	P	P	P	**G(5.46)**	P	P	P
Isopropanol:Water(1:1)	**G(5.73)**	**G(5.80)**	**G(6.20)**	**G(7.60)**	**G(3.10)**	**G(6.30)**	P
Propan-1,2-diol:Water(1:1)	**G(4.20)**	P	**G(4.50)**	**G(5.0)**	**G(2.10)**	P	**G(4.60)**
ACN:Water(1:1)	**G(1.86)**	P	P	P	P	P	P

Interestingly, **UTz 1–7** were found to gelate only propan-1, 2-diol, and acetonitrile with significantly low MGC values ranging from 1.70 % w/v to 8.60 % w/v to form an opaque gel. Surprisingly, all the compounds showed an excellent gelling ability towards a mixture of solvents rather than pure solvent (Table 3.1). It is important to note that solvents with high polarity or hydrogen bond-forming capability such as water, methanol, ethanol, etc. may influence the gelation process significantly[29–31]. The sol–gel transition (T_{gel}) temperature of compounds in three solvents namely, acetonitrile, Propane-1,2-diol, and water/isopropanol mixture, were carried out to find the stability of the gel. The observed increase of T_{gel} values with an increase in the

concentration of gelator to a certain concentration and then, levelling off is in line with reported sol– gel transition temperature behaviour with the variation of gelator concentration (Figures 3.1(a)-3.7(a)).

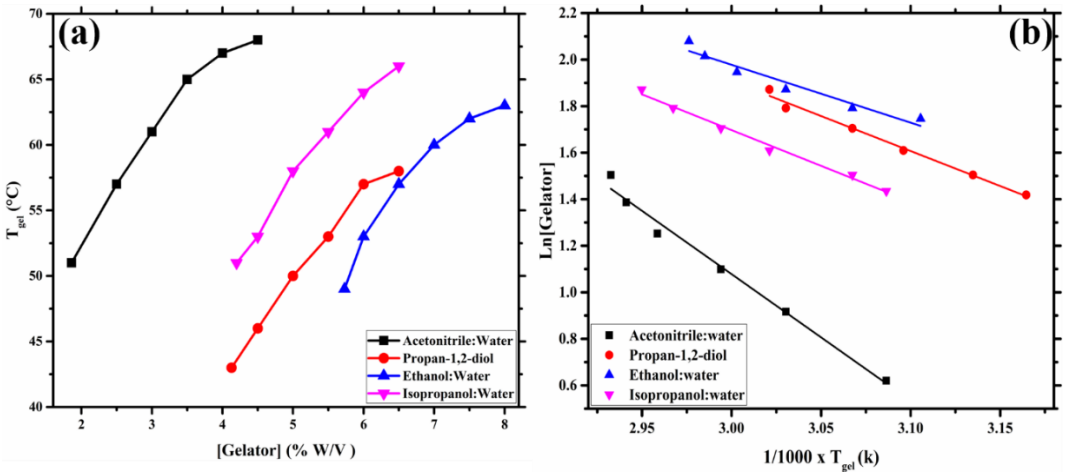

Figure 3.1 *(a) Plot of T_{gel} versus Gelator concentration (b) Linear plot of ln[Gelator] versus reciprocal of T_{gel} of UTz-**1***

Understandably, the increase in the number of gelator molecules (i.e., Increase in [Gelator]) strengthen the length, complexity, and entanglement of gelator fibers resulting in higher sol–gel transition temperature (higher stability) to certain limiting concentration. After reaching a particular gelator concentration (saturation) no further increase in the entanglement and stability of gelator fibers takes place, resulting in constant sol– gel transition temperature (T_{gel}). Furthermore, a semilog plot of gelator (Figure 1b–7b) concentration (in mole fraction) versus $1/T_{gel}$ (K^{-1}) was plotted for various solvent/ solvent mixtures to obtain the enthalpy of melting (ΔH_m) according to the Schroeder-van Laar equation (Eq. (4).) A linear relationship between gelator concentration and $1/T_{gel}$ support the first order transition of melting of gelator fibers. Interestingly, the ΔH_m of all compounds in acetonitrile (a highly polar solvent) displayed the minimum influence of increases in the aliphatic carbon chain of gelator molecules on the enthalpy of melting (21.71 kcal to 24.04 kcal). Whereas the maximum change in enthalpy of melting was observed for propane-1,2 -diol (17.33 kcal to 44.28 kcal). Understandably, the increase in the thermal stability (T_{gel}) in propane-1,2-diol with the increase in the alkyl chain (**UTz 1–5**) may be due to better interdigitation between the alkyl chain (or increase in van der Waals interactions) of gelators molecules in the solvent and then sudden decrease in enthalpy of melting with the increase in alkyl chain (**UTz 6–7**) may be attributed to decrease in solubility of these compounds in the polar solvent[32].

$$\ln [\text{Gelator}] = \Delta H_m / RT_{gel} + \text{constant} \qquad (4)$$

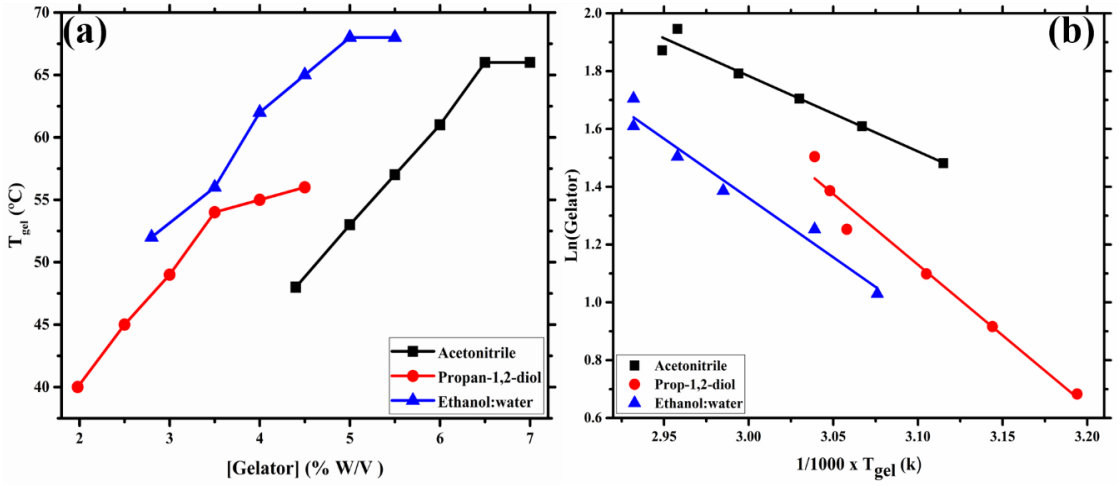

Figure 3.2 *(a) Plot of T_{gel} versus Gelator concentration (b) Linear plot of ln[Gelator] versus reciprocal of T_{gel} of* ***UTz-2***

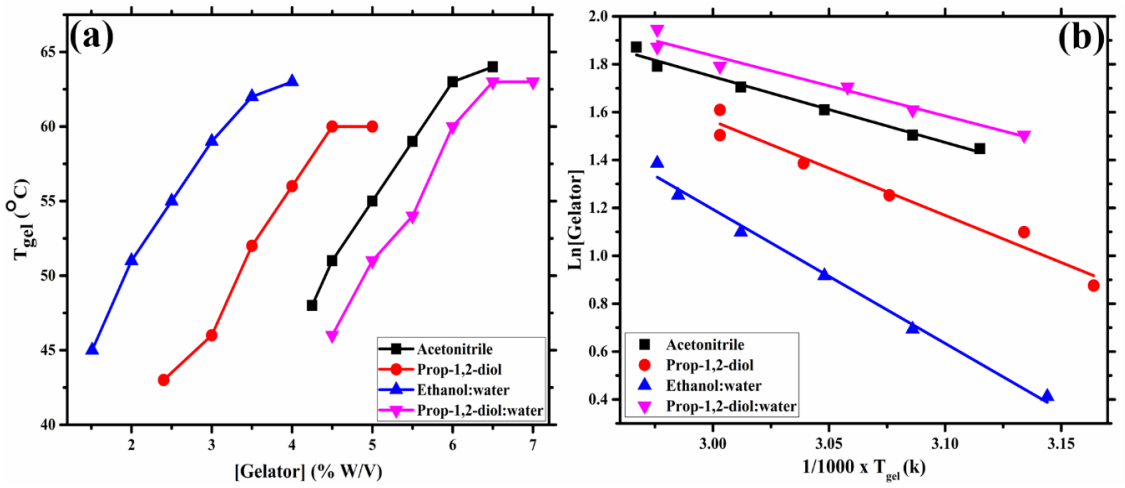

Figure 3.3 *(a) Plot of T_{gel} versus Gelator concentration (b) Linear plot of ln[Gelator] versus reciprocal of T_{gel} of UTz-**3***

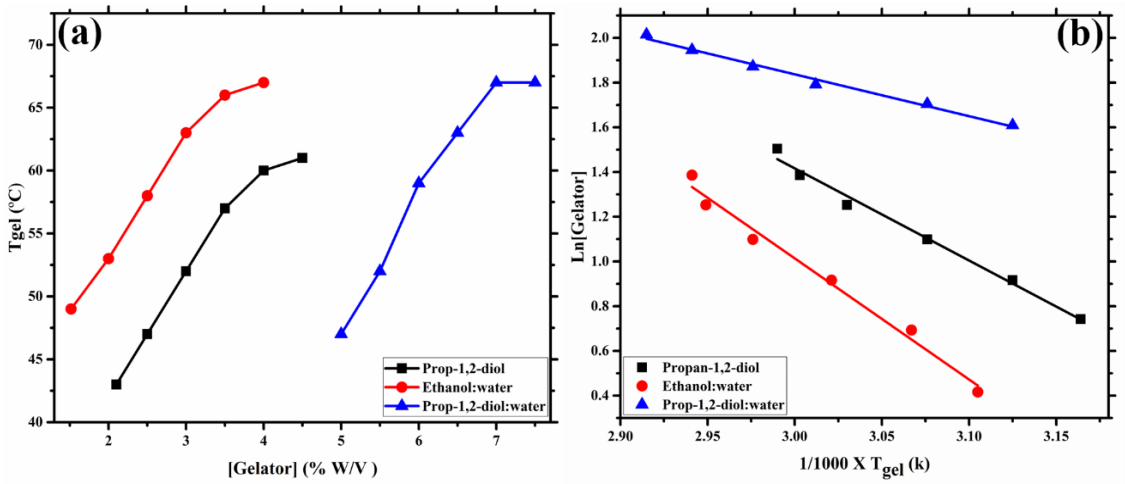

Figure 3.4 *(a) Plot of T_{gel} versus Gelator concentration (b) Linear plot of ln[Gelator] versus reciprocal of T_{gel} of UTz-**4***

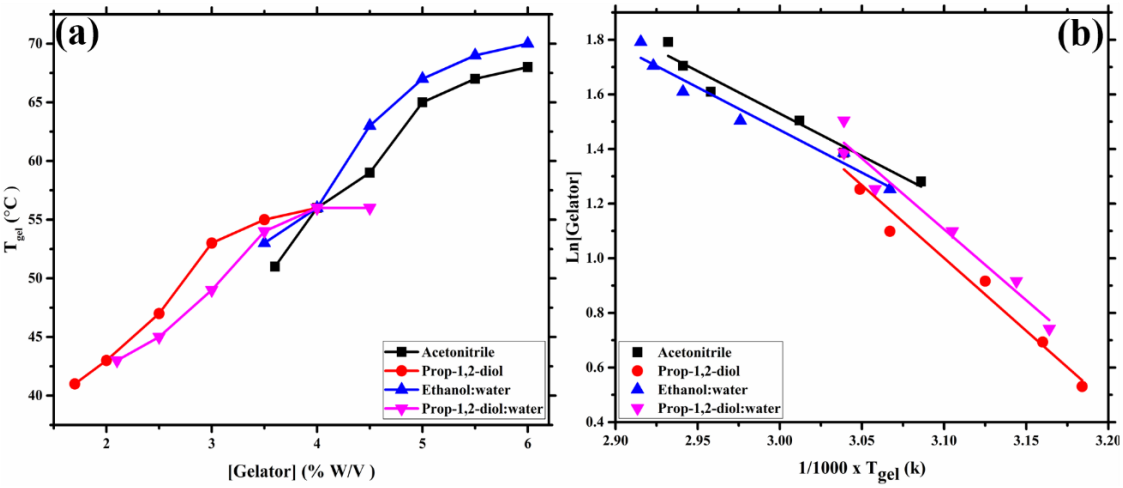

Figure 3.5 *(a) Plot of T_{gel} versus Gelator concentration (b) Linear plot of ln[Gelator] versus reciprocal of T_{gel} of UTz-**5***

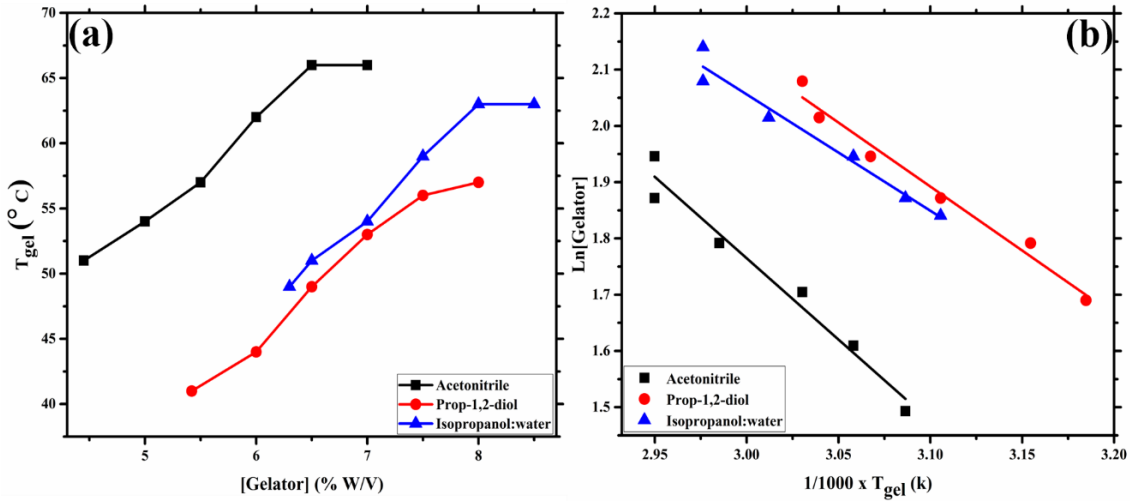

Figure 3.6 (a) *Plot of T_{gel} versus Gelator concentration (b) Linear plot of ln[Gelator] versus reciprocal of T_{gel} of UTz-**6***

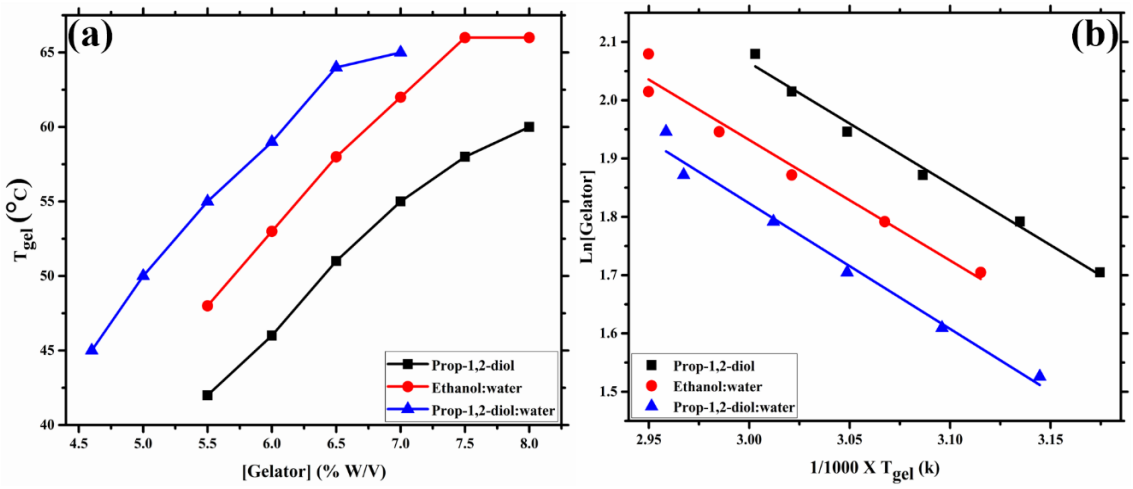

Figure 3.7 *(a) Plot of T_{gel} versus Gelator concentration (b) Linear plot of ln[Gelator] versus reciprocal of T_{gel} of UTz-**7***

Chain length	Propan-1,2-diol	Acetonitrile	Ethanol: water	Propan-1,2-diol: Water	Acetonitrile: water	Isopropanol: Water
11	25.00	-	20.68	-	45.19	25.53
12	40.66	21.71	34.11	-	-	-
13	32.72	22.83	46.53	20.89	-	-
14	34.36	-	45.04	15.56	-	-
15	44.28	25.82	25.94	43.16	-	-
16	18.90	24.038	-	-	-	17.19
18	17.33	-	17.19	17.90	-	-

Table 3.2 *ΔH_m Values(kJ/mol) extracted from the graph.*

3.4.2 Infrared spectroscopy studies

FTIR spectra are used extensively to ascertain the hydrogen bonding interaction as several absorptions bands in the infrared region show distinct shifts with hydrogen bonding[33]. In the present study, FTIR spectra of all compounds (**UTz 1-7**) in solid-state displayed characteristic bands such as between ~3360-3225 cm^{-1} corresponding to the symmetric -NH stretching vibrations[34] and band between ~2900-2845 cm^{-1} characteristic of -CH_2 Symmetric and anti-symmetric modes of hydrocarbon chains, respectively[35]. To address the possibility of change in the hydrogen bonding pattern with the formation of xerogel (dried gel), FTIR spectra of xerogel all compounds prepared from different solvents were also recorded.

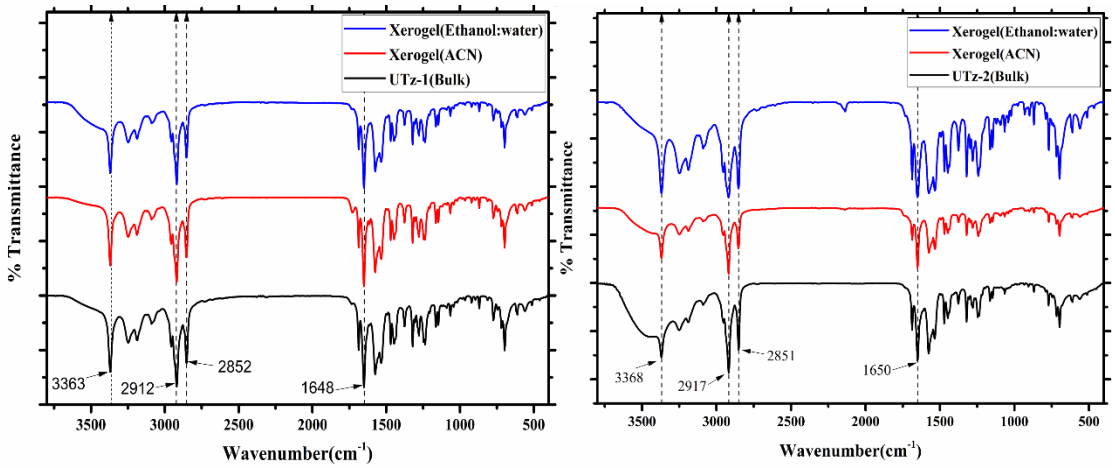

Figure 3.8 *IR Spectra of UTz-**1**(a) and UTz-**2**(b) and its respective xerogels*

Interestingly, almost superimposable spectra of xerogel and bulk solid suggest retention of hydrogen bonding pattern in both states. (Figures 3.8-3.11). Furthermore, our attempt to record IR spectra of native gel form in various solvents was unsuccessful due to the strong absorption of solvent molecules in the gel state.

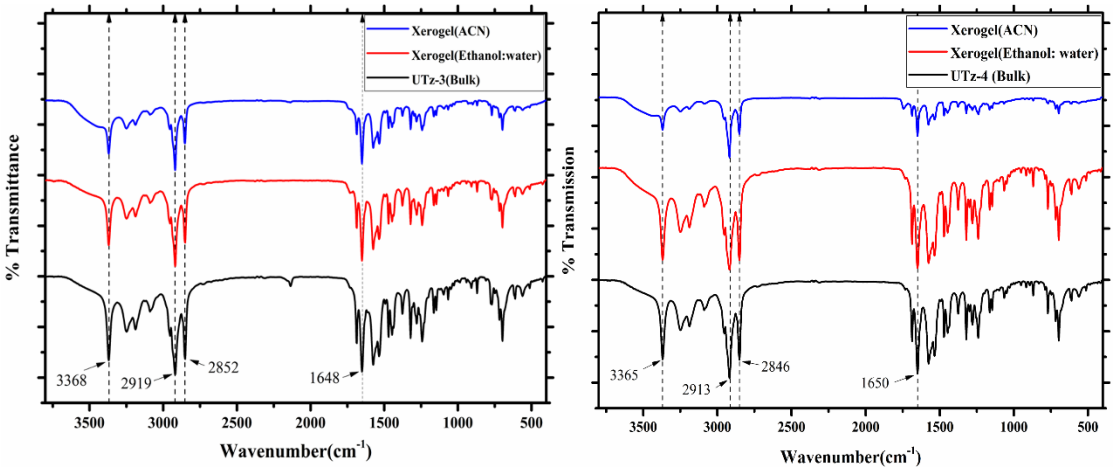

Figure 3.9 *IR Spectra of UTz-3(a) and UTz -4(b) and its respective xerogels*

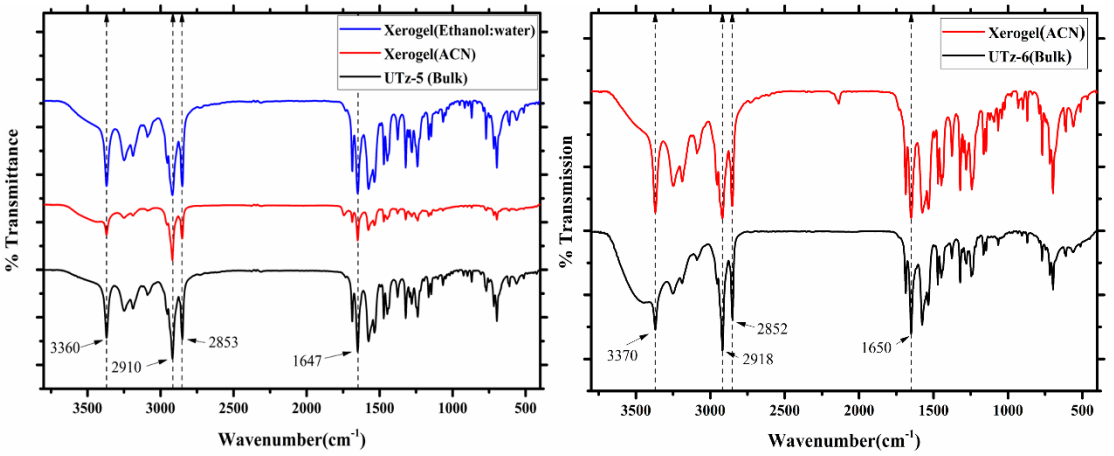

Figure 3.10 *IR Spectra of UTz -5(a) and UTz -6(b) and its respective xerogels*

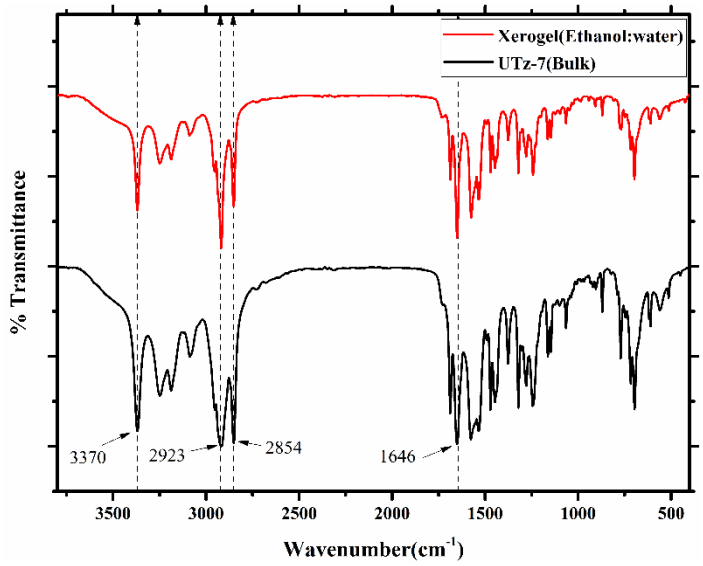

Figure 3.11 *IR Spectra of UTz -7 and its xerogel*

3.4.3 Rheological studies

To evaluate the deformation behaviour of gel samples, strain sweep experiments were carried out on gel samples of **UTz 1-7**. Figures 3.12-3.15 represents the change in storage modulus (G') and loss modulus (G") as a function of oscillation strain. In Rheological measurements of gels, the storage modulus (G') is almost an order greater than G" (loss modulus) (except for **UTz 2**) indicates the formation of a strong viscoelastic gel.

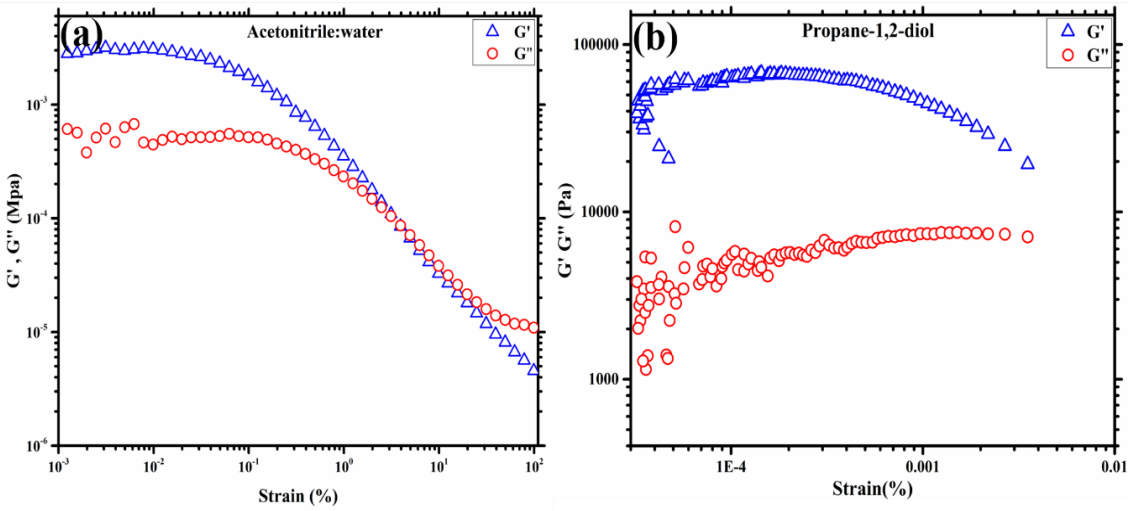

Figure 3.12 *Evolution of G' and G" as a function of oscillation strain of UTz -**1**(a) 1.86% in Acetonitrile: Water (b) 4.2 % in Propane-1,2-diol.*

The solid-like property of all compounds changes to more liquid-like property at the crossover point of G' and G" when subjected to strain amplitude of 1% at an oscillation strain of ~10 %. Furthermore, to understand how the increase of alkyl chain (decyl to heptadecyl) influences the gelation phenomenon, rheological measurements were carried out on the **UTz (2–7)** in the same solvent i.e., propane-1,2-diol (Figures 3.14-3.16). All the compounds show typical viscoelastic behaviour of gels as evident from figures and their data is summarized in Table 3.3.

Table 3.3 *Rheological parameters of Propane-1,2-diol*

Compound	Storage modulus(G')(Pa)	Loss modulus(G")(Pa)	G'/G"	Cross over
UTz-**1**	20810.77	3581.37	5.8	0.116
UTz-**3**	50324.21	32991.72	10.6	0.990
UTz-**4**	49073.50	4037.31	12.1	3.127
UTz-**5**	13377.92	1218.03	10.9	1.089
UTz-**6**	55666.84	9859.23	5.6	0.004
UTz-**7**	19034.26	3013.38	6.3	0.010

As evident from the table, in all the cases G' is almost 5 times G" and the strongest gel was a gel of **UTz-4** with the highest cross-over point among all the compounds at 3.127. The result suggests the enhancement of gelation property with the increase of the alkyl chain when the solvent remains the same.

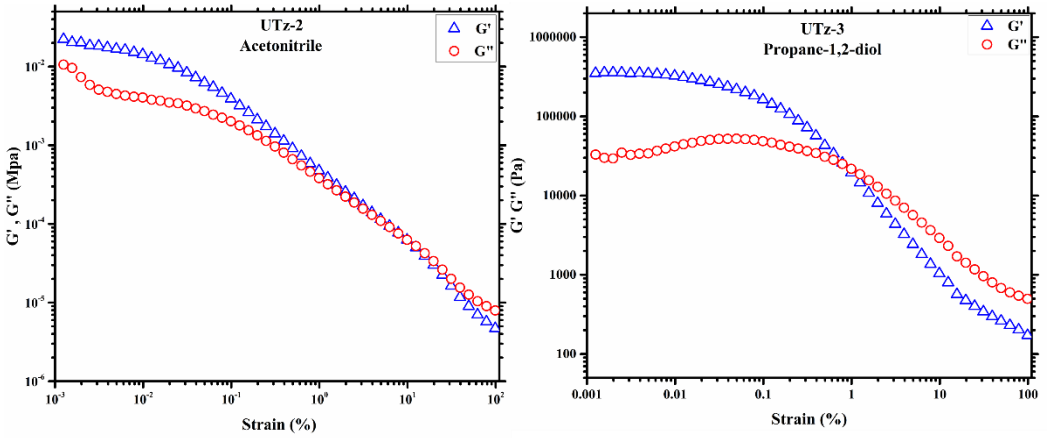

Figure 3.13 *Evolution of G' and G" as a function of oscillation strain (a) UTz -**2** in Acetonitrile (4.4 %) (b) UTz -**3** in Propane-1,2-diol (2.4%)*

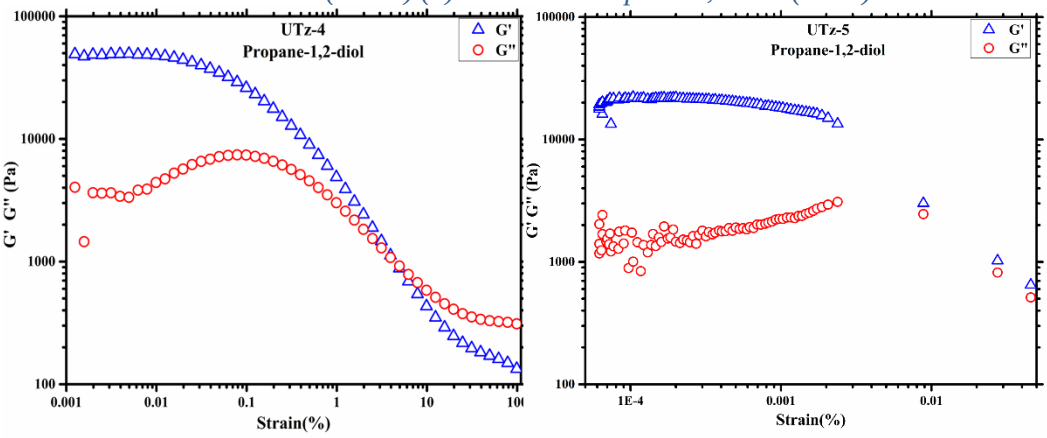

Figure 3.14 *Evolution of G' and G" as a function of oscillation strain (a) UTz-**4** in Propane-1,2-diol (2.1 %) (b) UTz -**5** in Propane-1,2-diol (1.7%)*

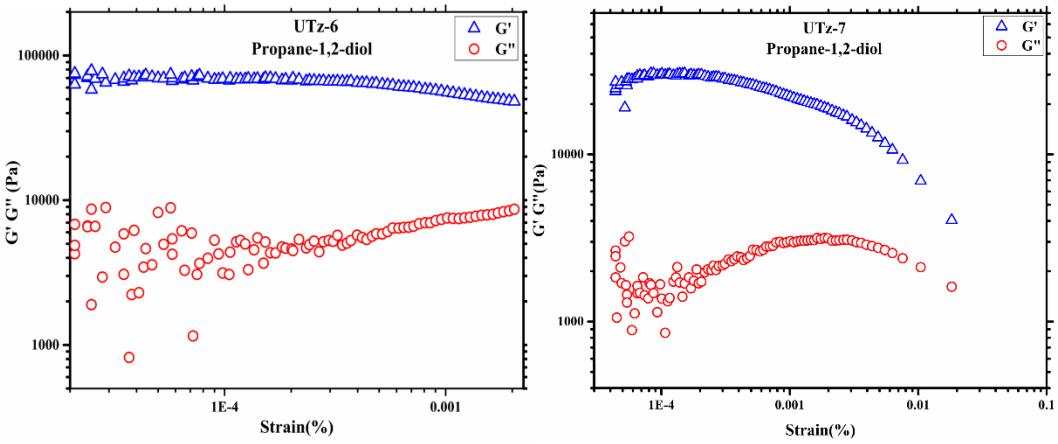

Figure 3.15 *Evolution of G' and G" as a function of oscillation strain (a) UTz -**6** in Propane-1,2-diol (5.4 %) (b) UTz -**7** in Propane-1,2-diol (5.5%)*

3.4.4 Morphological Studies

Morphology of various gelator fibers was probed using POM (Polarised optical microscope) and SEM(Scanning electron microscope) as they reveal the nature of gelator fibers (xerogel) from a micrometer scale to nanometres[36–38]. POM images of **UTz 1–5** in various solvents displayed very fine randomly distributed fibrous crystals [See Figure 3.16].

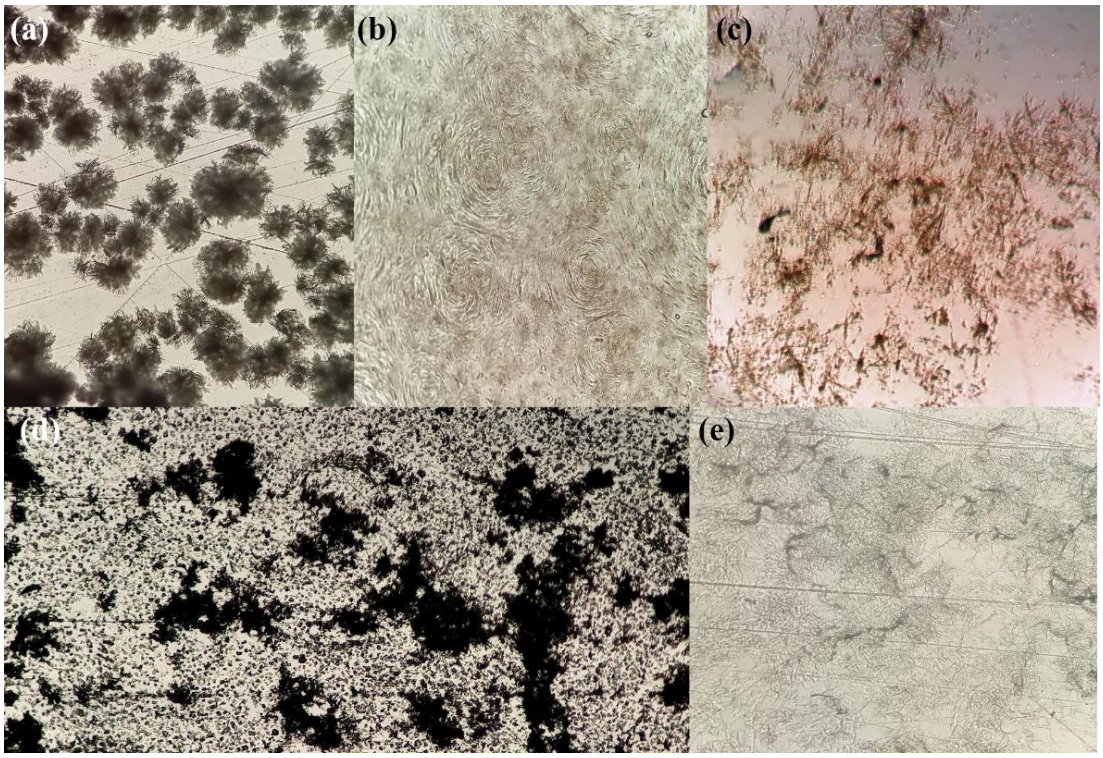

Figure 3.16 *POM images of (a) UTz -**5** in acetonitrile, (b) UTz -**5** in propane-1,2-diol (c) UTz -**3** in propane-1,2-diol, (d) UTz -**1** in propane-1,2-diol, (e) UTz-**2** in ethanol:water*

Surprisingly, the micrographs of **UTz-1** in acetonitrile: water and ethanol: water displayed different morphology [See Figure 3.17 (a&b)]. SEM image of xerogel of **UTz-1** in acetonitrile: water is a more complex microstructure aggregate of gelator fibers, whereas, in the solvent mixture ethanol: water xerogel image appeared 2-D sheet-like morphology. Interestingly, compounds **UTz-2**, **3**, and **5** displayed similar 2-D structures in various solvents [Figure 3.17c-3.17e]. SEM image of xerogel without a definite fibrillar structure suggests the random arrangement of the alkyl chain which was further supported by the experimental results obtained using Powder X-Ray diffraction (PXRD) and SANS.

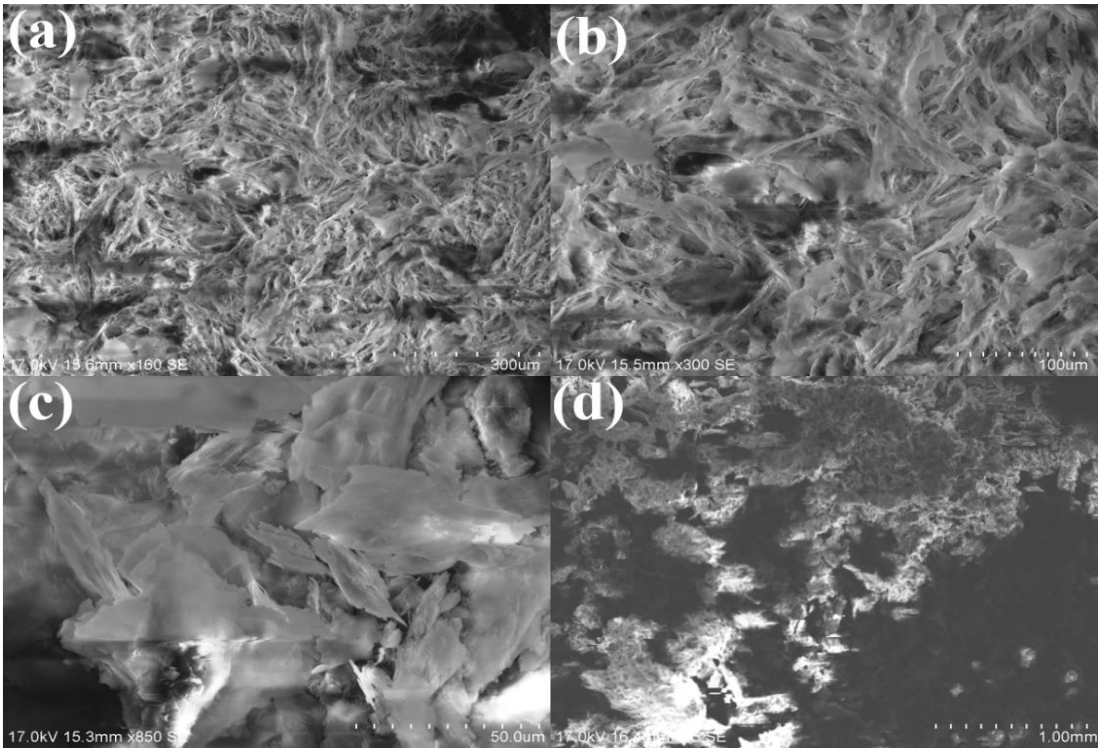

Figure 3.17 *SEM images of Xerogel of UTz -**1** in (a, b) acetonitrile: water, (c, d) ethanol: water*

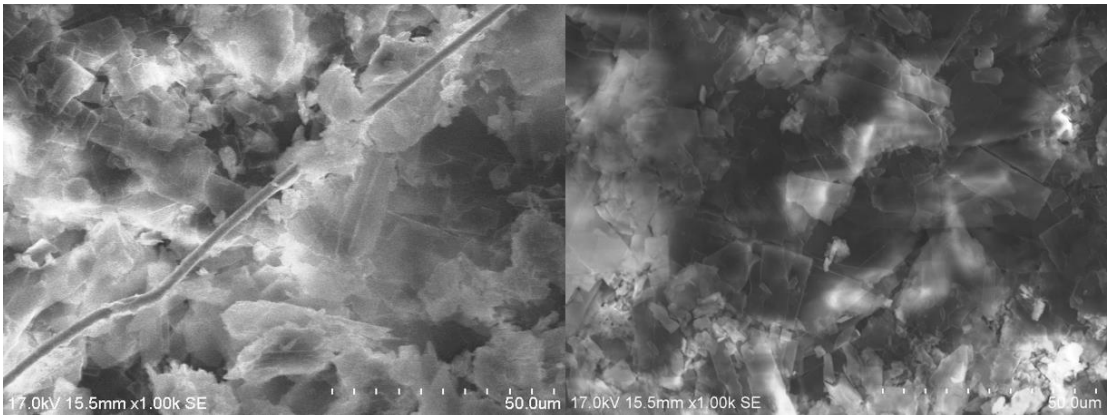

Figure 3.18 *SEM images of Xerogel of UTz-**2** in ethanol: water*

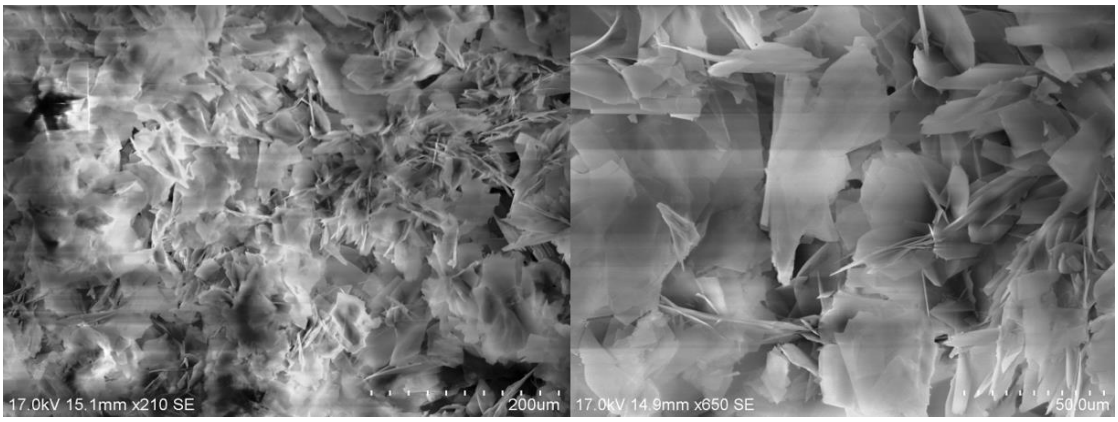

Figure 3.19 *SEM images of Xerogel of UTz-**3** in ethanol: water*

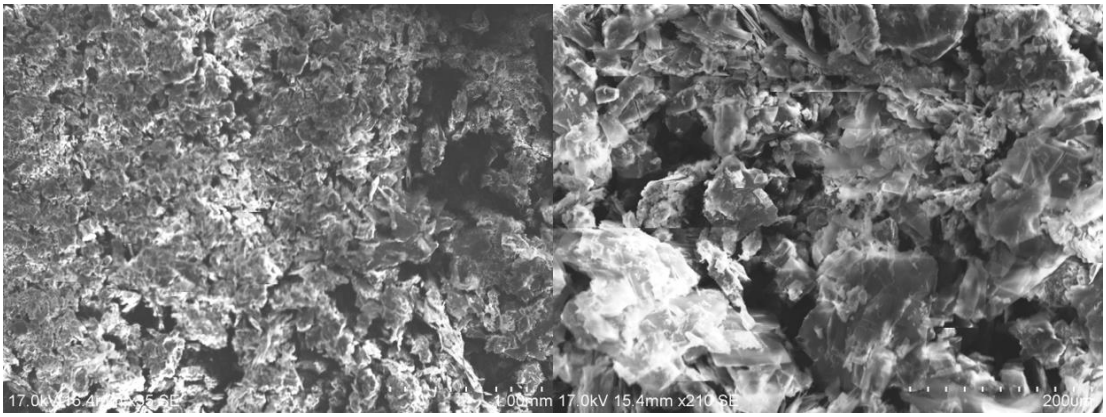

Figure 3.20 SEM images of Xerogel of UTz-5 in acetonitrile

3.4.5 Powder XRD Studies

Powder XRD is frequently employed to understand the probable packing arrangements of gelator molecules in the xerogel (dried gel) and bulk solid and compare it with simulated Single Crystal structure (if available). It is always difficult to extrapolate the packing of molecules in the solid state with the packing of molecules in a metastable gel state. However, the methodology developed by Weiss and his group[39], proved to be beneficial to get an insight into the probable packing of molecules in a xerogel state if the PXRD of xerogel (dried gel) matches perfectly well with simulated Single-crystal X-ray structure packing[39,40].

In the present study, we have recorded powder XRD patterns of **UTz-1,2,** and **5** as bulk solid and xerogel obtained from different solvents [Figure 3.21-3.22]. Most of the peaks in PXRD in bulk and xerogel showed a reasonable match in all the studied compounds (bulk and xerogel).

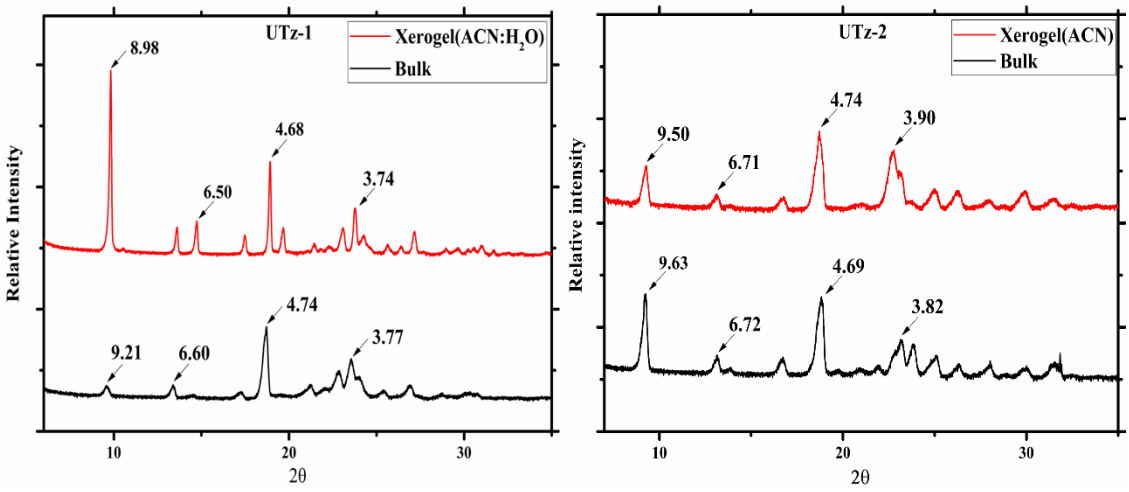

Figure 3.21 Powder XRD of UTz-1 and UTz-2 with the corresponding xerogel in respective solvents.

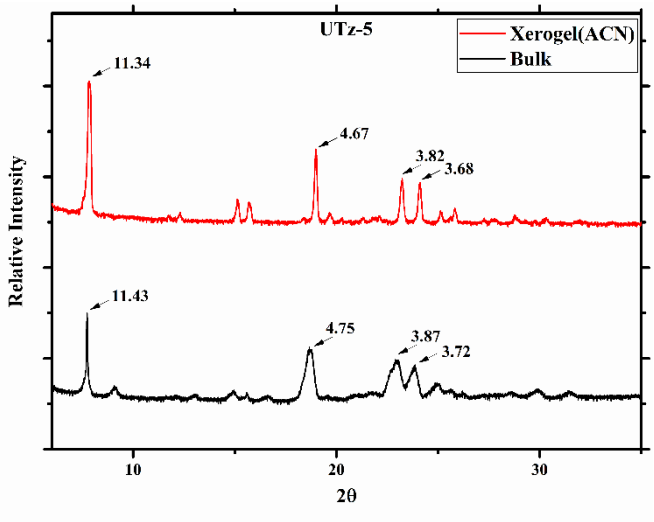

Figure 3.22 Powder XRD of UTz-5 with the corresponding xerogel

Unfortunately, we couldn't obtain any single crystal in this series of compounds to make a decisive comment about the packing of molecules in solid (bulk) and xerogel states. It is important to note that PXRD (bulk solid and xerogel of **UTz-1** and **5**) show sharp peaks at d-spacing 3.7 Å and 4.6 Å suggesting the presence of π-π stacking and alkyl chain interdigitation (van der Waals interaction), respectively[40]. Interestingly, gelator **2** displayed a peak position corresponding to d-spacing 3.9 Å (xerogel) and 3.8 Å (bulk solid) presumably due to weak van der Waals interaction between the alkyl chain[41]. However, the packing of molecules in a dried state and metastable gel state is frequently found to be different. So, information obtained from xerogel (dried gel) PXRD may not be conclusive, but indicative of the probable interactions presents in the gel state.

3.4.6 Density functional theory studies

Thiazole containing urea derivatives are known to show two types of conformation syn-syn and anti-syn[42], as shown in Scheme 3.4, depending upon the solvent of crystallization (solvents may stabilize the particular conformation)[43,44].

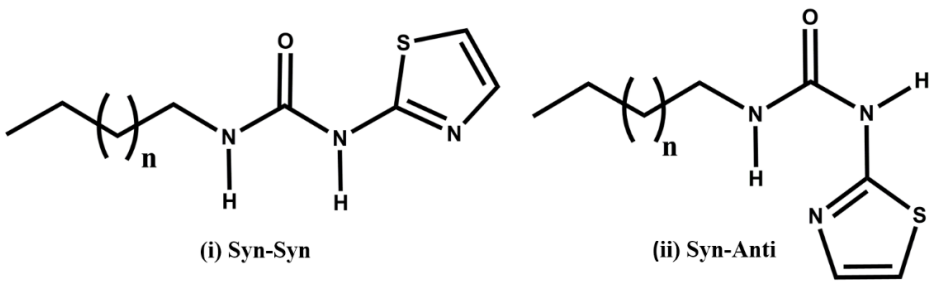

Scheme 3.4 Probable conformation of UTz 1–7.

In the absence of SCXRD (Single-crystal X-ray diffraction) of synthesized gelators, we decided to probe the optimized geometry of the gelator molecule and its dimer to get an insight into the hydrogen bonding pattern (Supramolecular synthons) and their conformational preference using computational methods. The optimized geometry dimer of thiazole-based urea, and may guide us to the probable arrangement of molecules leading to supramolecular assembly[45,46]. The geometry optimization and conformation analysis of all compounds were carried out by DFT calculations using B3LYP/6–31(d) basis sets[47]. The optimized geometry of **UTz-1**(Figure 3.23). and dimer of **UTz-1** are shown in Figure 3.24. The optimized geometry of **UTz-1** and its dimer displayed the anti-syn conformation of urea functional group.

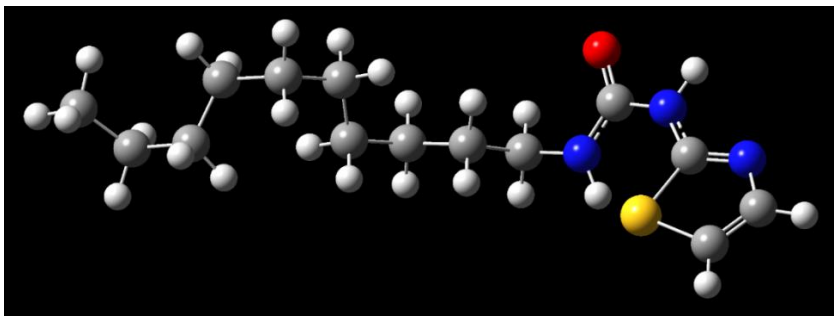

Figure 3.23 *Optimized structure of UTz-**1**(inset) obtained by DFT calculations using B3LYP/6–31(d) basis set*

The dimeric arrangement of **UTz-1** showed cyclic N-H···O supramolecular synthons with graph set $R_2^2(8)$ representation along with N-H···N intramolecular interaction, which matches well with the similar crystal structure[42,48].The conformational preference of anti-syn conformation over syn-syn conformation of urea functionality in compounds (**UTz 1–7**) may be attributed to the formation of intramolecular hydrogen bond [N-H···N(thiazole)].

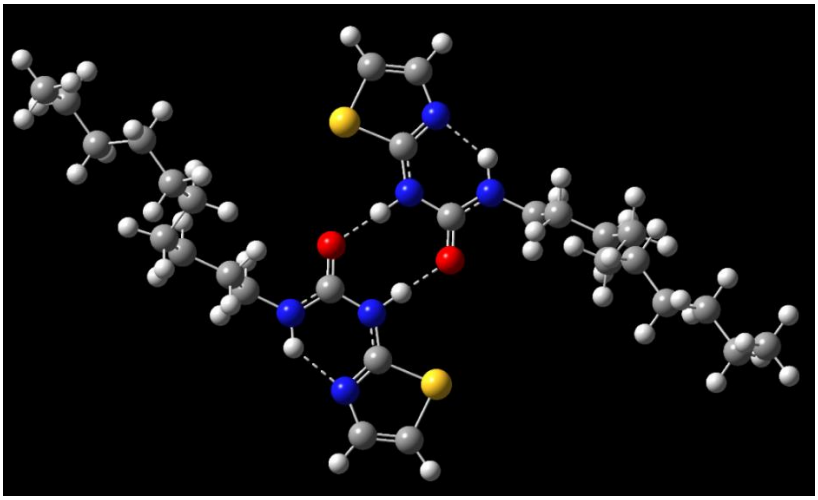

Figure 3.24 *Optimized structure of UTz-**1** dimer obtained by DFT calculations using B3LYP/6–31(d) basis set.*

Based on the reported crystal structure of thiazole-based urea derivatives and optimized geometry of **UTz-1**, we propose the formation of anti-syn conformation in **UTz 1–7** with extended alkyl chain in both directions (Scheme 3.5a). Furthermore, the dimeric structure of compound (**UTz 1–7**) may extend to 3-D supramolecular assembly, either by bifurcated hydrogen bond involving oxygen of a urea functional group and/or through various van der Waals interactions between extended alkyl chain (Scheme 3.5b).

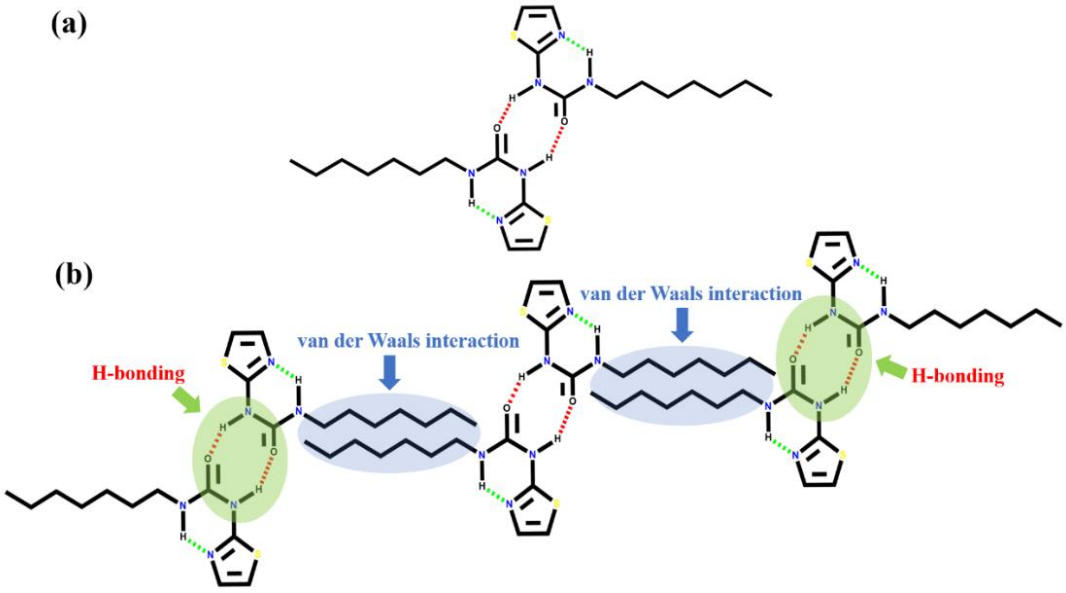

Scheme 3.5 *(a) Probable synthon for UTz-**1** (b) Extended hydrogen bonding in 3-D space*

3.4.7 Small-angle neutron scattering studies:

To extract the structural packing information in situ (in the native gel state) SANS study has the edge over any other characterization technique. As it is possible to carry out a SANS study in gel, solution, and solid-state to probe the packing of molecules from a few nanometres to a couple of hundreds nanometre scale[49,50]. A detailed SANS analysis was carried out to investigate the packing of gelator molecules in gel/solution/solid-state. Interestingly all the powdered (solid) samples show the same shape in the log–log plot as shown in Figure 3.25. Unfortunately, one of the samples (**UTz-2**) doesn't give sufficient scattering in solid-state but strong scattering was observed for **UTz-2** in gel state.

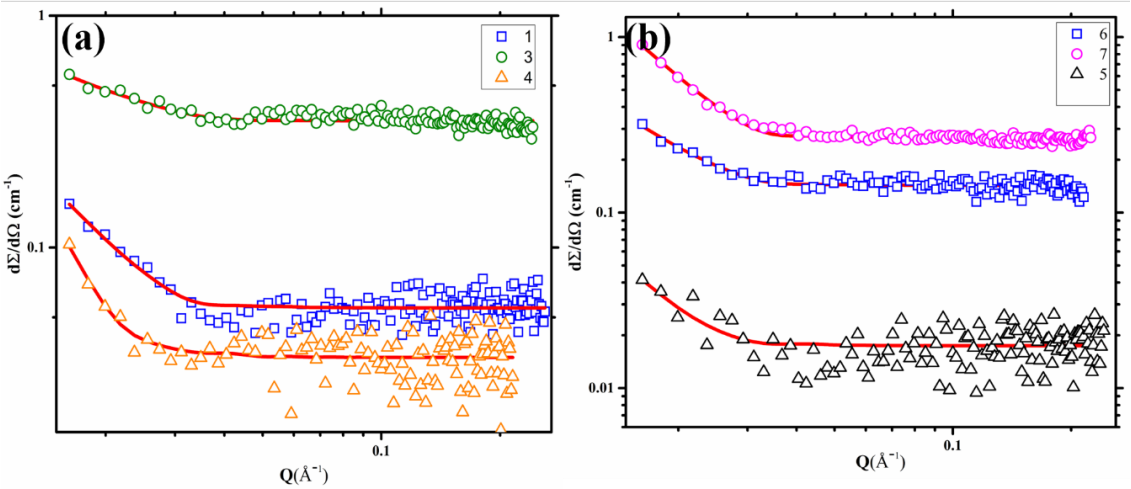

Figure 3.25 *SANS profile for Powdered (a) UTz **1,3** and **4** (b) UTz **5,6** and **7** where red line indicated the best fitting*

Several fitting methods were used to fit the scattering data and it was found to be best fitted with the long cylindrical model and their cross-sectional radii are summarized in Table 3.4. Here continuous red line in the figure represents the best fitting to the data. Furthermore, data were also collected from the different selected gel samples (**UTz 1, 2** and **5**) with varying temperatures, to probe the primary structure of the fibrils. Out of 6 compounds analyzed for solid-state SANS scattering, three were selected for further study and to get an insight into packing in solid-state and gel states. A SANS scattering data of powder and gel-state for gelators **UTz-1** and **UTz-5** were recorded and analyzed, the packing in the native solid-state and the gel state appeared to be quite different. (Figure 3.26)

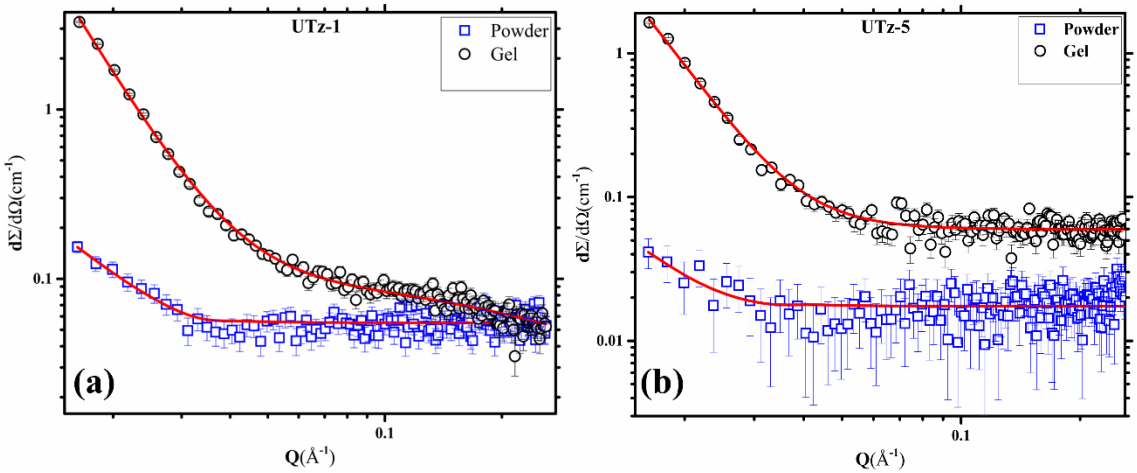

Figure 3.26 *A comparative SANS profile of UTz-**1** and UTz-**5** in powder(bulk) and gel state in acetonitrile: water mixture and Acetonitrile respectively*

The native powder of compounds **UTz-1** and **UTz-5** displayed the long cylindrical packing with a cross-sectional radius approximately equal to 117.86 Å and 113.87 Å, respectively, whereas the packing of molecules in the gel state couldn't be fitted with the definite shape. Therefore, scattering data of gel (**UTz-1**, **2** and **5**) were analyzed using a traditional two-stage network of gels[25,51,52] and interestingly, similar 2-D sheet-like morphology was also observed in SEM analysis of various xerogel (Figure 3.17). Furthermore, to explore change in packing of molecules (**UTz-1**, **2**, and 5) in the sol and gel phase, variable temperature experiments were carried out on **UTz-1** in ACN: water gel and gelators **UTz-2** and **UTz-5** in ACN gel (Figure 3.27). As expected, data intensity decreases with the gradual increase in temperature representing the loosening of gelator assembly with the increase in temperature. In the case of **UTz-1** and **UTz-2** scattering changes at a certain temperature (typically Tgel values), the plot show the change of unspecific cluster with the correlation length of 40.9 Å and 55.5 Å to the cylindrical dimension with a cross-sectional radius of 93.5 Å and 86.6 Å respectively (Table 3.5).

Table 3.4 *Cross section radii extracted from the fitting Scattering of data of Bulk*

Compound	Cross sectional radii(Å)
UTz -1	117.86
UTz -2	No scattering
UTz-3	77.64
UTz-4	142.34
UTz-5	113.87
UTz-6	93.49
UTz-7	102.06

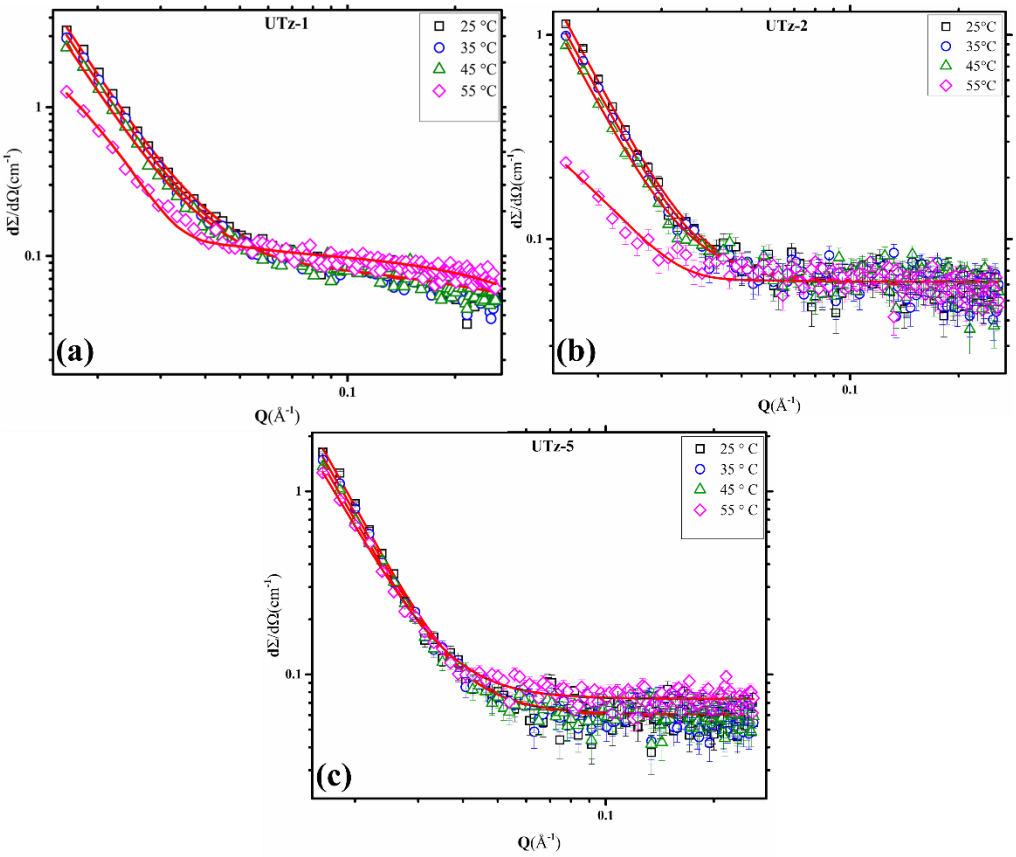

*Figure 3.27 SANS profile of gelator **UTz-1**, **2** and **5** at various temperature, here red plain line indicates the best fitting to the scattering data*

Gelator **UTz-5** shows different behaviour from gelators **UTz-1** and **UTz-2**, its SANS profile remains the same throughout the experiment with the change in the correlation length from 51.0 Å to 55.8 Å, and with a decrease in the fractal dimension depicts the loosening of the gel structure.

Table 3.5 Dimension data obtained from fitting (Ornstein–Zernike + Mass fractal) of SANS scattering data

Compounds	Temperature(˚C)	Correlation length(Å)	Fractal dimension (D_m)
UTz -1	25	40.9	2.98
	35	44.3	2.97
	45	44.9	2.97
	55	Cross-sectional radius of cylinder, R_{cr} = 93.5 Å	
UTz -2	25	55.5	2.50
	35	56.8	2.45
	45	70.6	2.36
	55	Cross-sectional radius of cylinder, R_{cr} = 86.6 Å	
UTz -5	25	51.0	2.64
	35	51.9	2.60
	45	53.5	2.60
	55	55.8	2.58

3.4.8 Anion sensing studies

LMOGs are frequently being used as anion sensors[15,53–57], as removal of toxic industrial waste[58–60], and are popular due to their response to the external stimuli[53,61,62], especially gelators having hydrogen bonding sites such as thiazole[63] and urea functionality are probed due to their high selectivity and sensitivity towards fluoride, chloride, sulphate and acetate ions[12,64,65]. Inspired by the earlier reports, we decided to explore the potential of the present series of compounds (**UTz 1–7**) as anion sensors.

Various salts such as tetrabutylammonium salts of fluoride, bromide, chloride, hydrogen sulphate, iodide, and hexafluorophosphate, were titrated in tetrahydrofuran (THF) solvent against the synthesized series of urea-thiazole compounds to examine their anion binding capability. Surprisingly, out of various halides, sulphates, and hexafluorophosphate used in the present study, only iodide ions showed very high selectivity towards **UTz-1**. It displays an absorption peak at 255 nm which decreases upon the addition of iodide, with the formation of a new peak at 292 nm with an isosbestic point at 265 nm, clearly confirming the formation of new complex species (Figure 3.28a). The new peak at 292 nm of iodide urea complex was found to depend upon the iodide concentration.

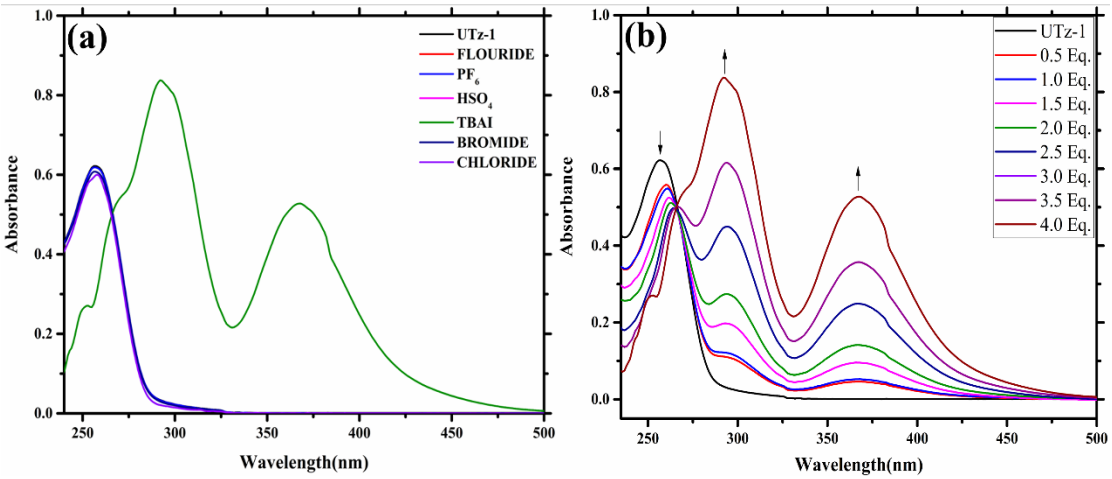

Figure 3.28 *UV–Visible absorption spectra of UTz-**1**(50 μM) in THF (a) With 4 equivalents of various Tetrabutylammonium salts. (b) Change in UV–Visible with addition of Tetrabutylammonium iodide in THF solvent*

No such change in peak position (or new peak formation) was observed in the case of fluoride, chloride, sulphate, and hexafluorophosphate ions during titration (Figure 28a). No selectivity towards sulphate, chloride and fluoride ions further supported that confirmation of thiazole urea compounds is syn-anti as observed in related crystal

structures and optimized geometry of dimer of **UTz-1**; as it is well established that syn-syn conformation of urea favours binding with chloride and fluoride ions[12].

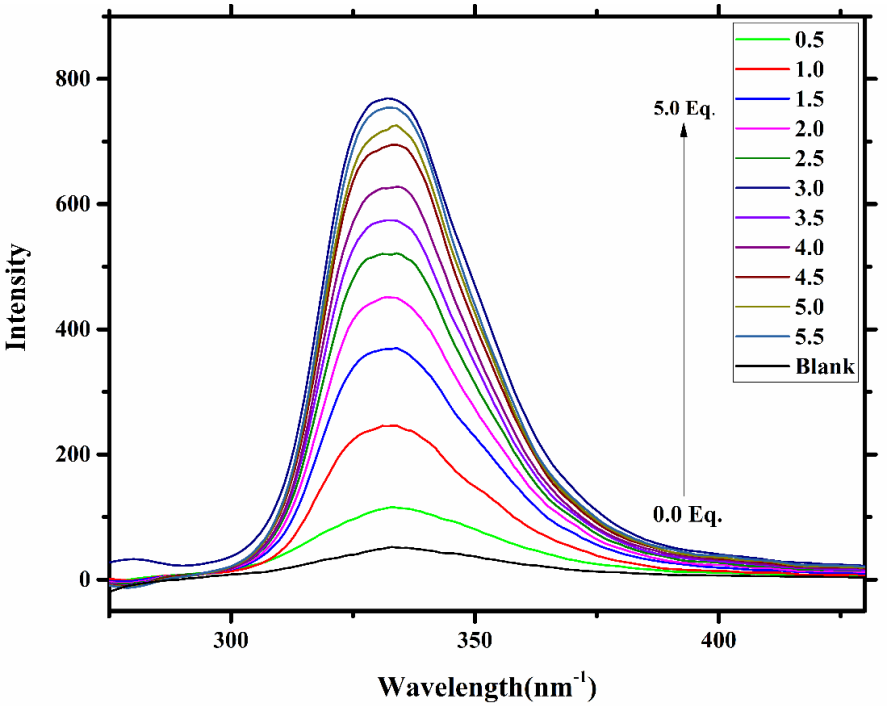

Figure 3.29 *Emission spectra of UTz -**1**(50 μM) in THF with gradual increase in the Tetrabutylammonium iodide concentration*

Apart from the UV–Visible spectra, the Emission spectra of **UTz-1** were also recorded with an excitation at 298 nm with the increasing concentration of iodide. Initially, **UTz-1** displayed a very weak emission peak at 333 nm which gradually increases with addition of TBAI solution in THF. The intensity of emission peak at 333 nm was observed to enhance almost 10 times with addition of 5 equivalent of iodide salt (Figure 3.29). Furthermore, Job's plot was used to establish the composition of complex formed between **UTz-1** and iodide ion (Figure 3.30a). The composition of iodide ion with **UTz-1** complex is found to be 1:1, which further establish why it is not able to sense Cl^-/F^-ion (complex of Cl^-/F- ion with urea compounds requires 1:2 M ratio). The detection limit of iodide ion with **UTz-1** is found to be 0.133 mM. Detection limit was calculated from the calibration curve obtain by titrating **UTz-1**(50 Micromolar) with different concentration of TBAI in tetrahydrofuran as shown in figure 3.30b.

The detection limit was calculated using following formula and slope was calculated from the graph.

$$3.3\ \frac{SD}{SLOPE}$$ Where SD is Standard deviation

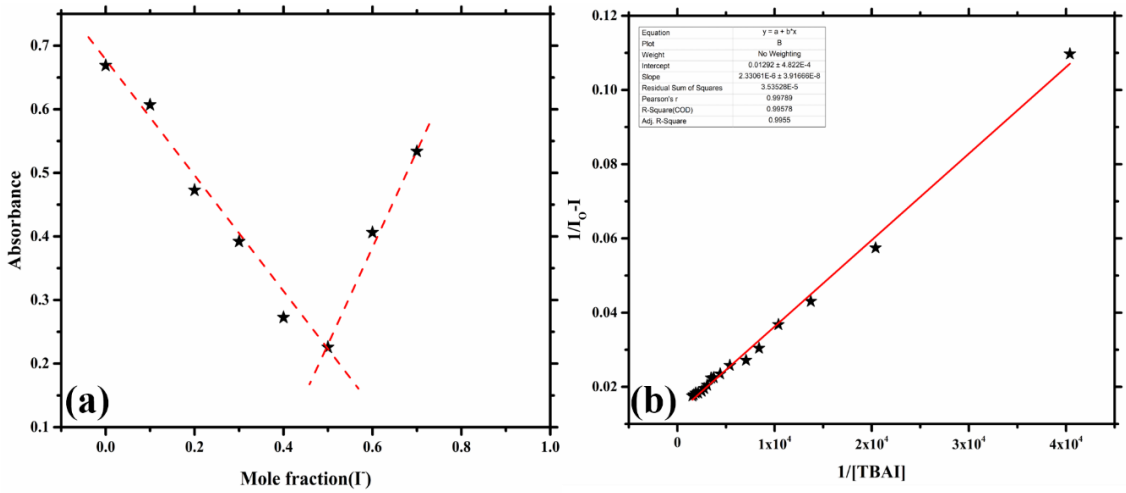

Figure 3.30 *(a) Jobs plot for the determination of stoichiometry of UTz-**1** with iodide (b) Detection limit calculation of UTz-**1***

The very high selectivity of iodide ion towards **UTz-1** in the solution phase (THF) prompted us to explore its effect on the gel phase. A high concentration of powder tetrabutylammonium iodide (TBAI) (3 equivalents) was added to the upper layer of preformed gel (acetonitrile: water system) in a test tube.

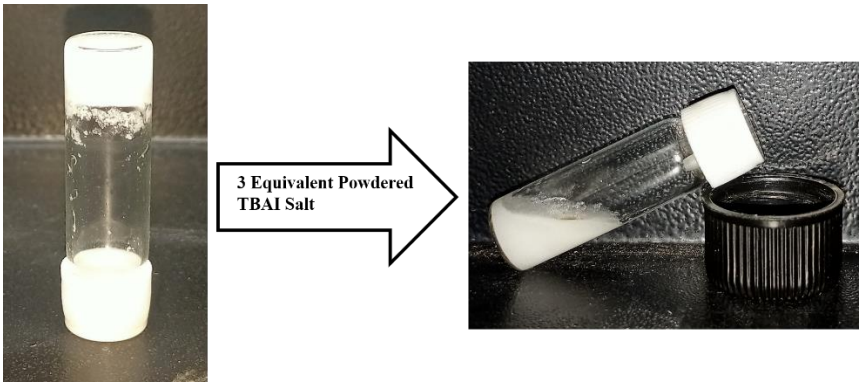

Figure 3.31 *Degelation after 3 equivalents of powdered TBAI salt was added to upper layer of gel*

Degelation or breaking of the gel was observed after 10 minutes (Figure 3.31), a schematic representation of probable mechanism of gel formation and breaking in presence of iodide ion is presented in Scheme 6. It is important to note that Ghosh et al. reported the pyridyl-urea capable of detecting the iodide anion through colour change with no phase transition[66] and Shen et al. reported Ag(I) hydrogel for selective detection through gel-sol transition[67].

In the present study, degelation was observed through naked eyes only in the presence of an iodide anion. Understandably, degelation implies that the self-assembly of **UTz-**

1 was greatly affected by the presence of iodide salt[54]. Visual detection of breaking of gel with the presence of iodide ion and very high selectivity and sensitivity towards iodide ions even in presence of chloride and fluoride ion in a urea-based compound is fascinating. Iodide detection and quantification are crucial due to their key role in physiological growth and functioning of the thyroid gland in humans[68].

Moreover, to understand the mechanism behind iodide ions sensing (not chloride and fluoride) and to probe the interaction between the **UTz-1** with Iodide ion using ^{1}H NMR spectroscopy. ^{1}H NMR spectra were recorded before and after addition of TBAI salt at different concentration (0.5, 1.0 and 2.5 equivalent). ^{1}H NMR of **UTz-1** with two types of NH proton of urea functionality (Designated as H_a and H_b, (Figure 3.32) is expected to interact proton with the solvent) without addition of iodide ion. NH_a proton was found to be shifted upfield with the gradual decrease in the intensity with an increase in the iodide ion concentration. The interaction of N-H proton with iodide ion supports the mechanism proposed for gel formation and breaking of gel. Understandably, the basic building block of **UTz-1**, i.e., dimeric unit, governed by intermolecular N-H···O interaction (scheme 4a), breaks down with addition of iodide ion, resulting into breaking of gel (see scheme 3.6).

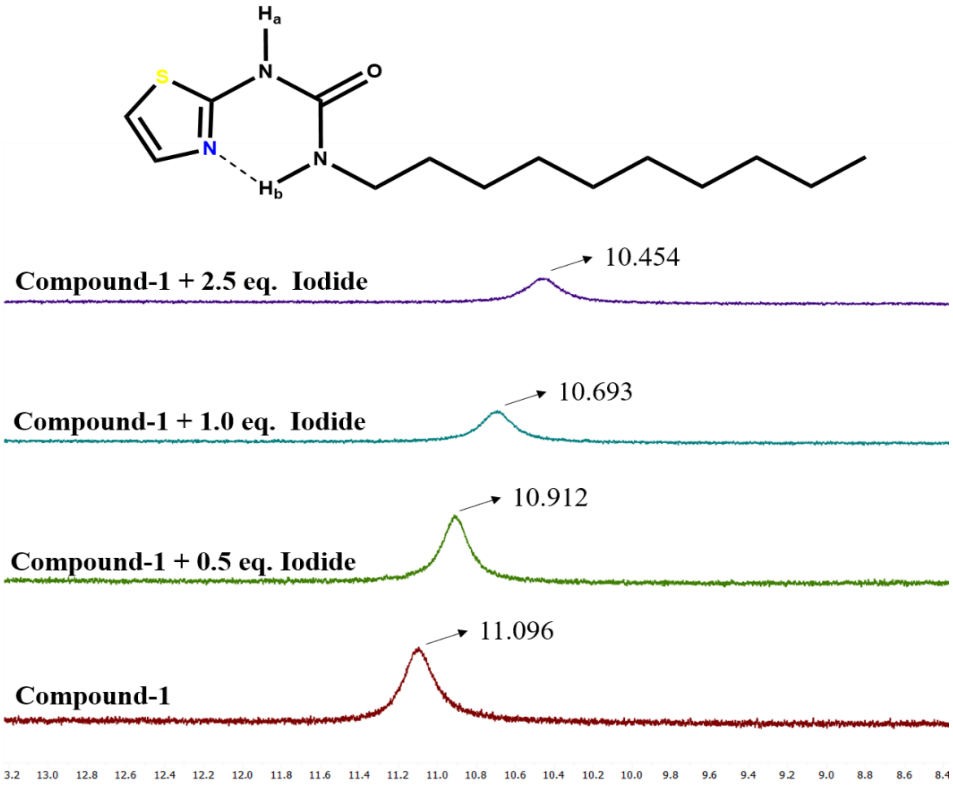

Figure 3.32 *^{1}H NMR (400 MHz) of UTz-1 in the presence of different concentration of iodide in $CDCl_3$*

Based on the information obtained from computational studies, SANS, PXRD, and NMR spectroscopy of **UTz-1** we proposed probable self-assembly of molecules in solid, liquid, and gel states. We believe **UTz-1** form a cylindrical assembly in solid-state (as observed in the solid-state SANS study) with a syn-anti conformation of thiazole moiety. The cylindrical assembly is lost in the gel phase due to multiple van der Waals interactions between the alkyl chain leading to a 2-D sheet-like structure as observed in SEM and SANS. The degelation of gel with iodide ion prompted us to propose the breaking of N-H···N and N-H···O hydrogen-bonded and formation of N-H···I^- interaction observed in NMR spectroscopy. A schematic representation of the hydrogen-bonded network in gel and degelation with the addition of iodide ion is shown in scheme 3.6.

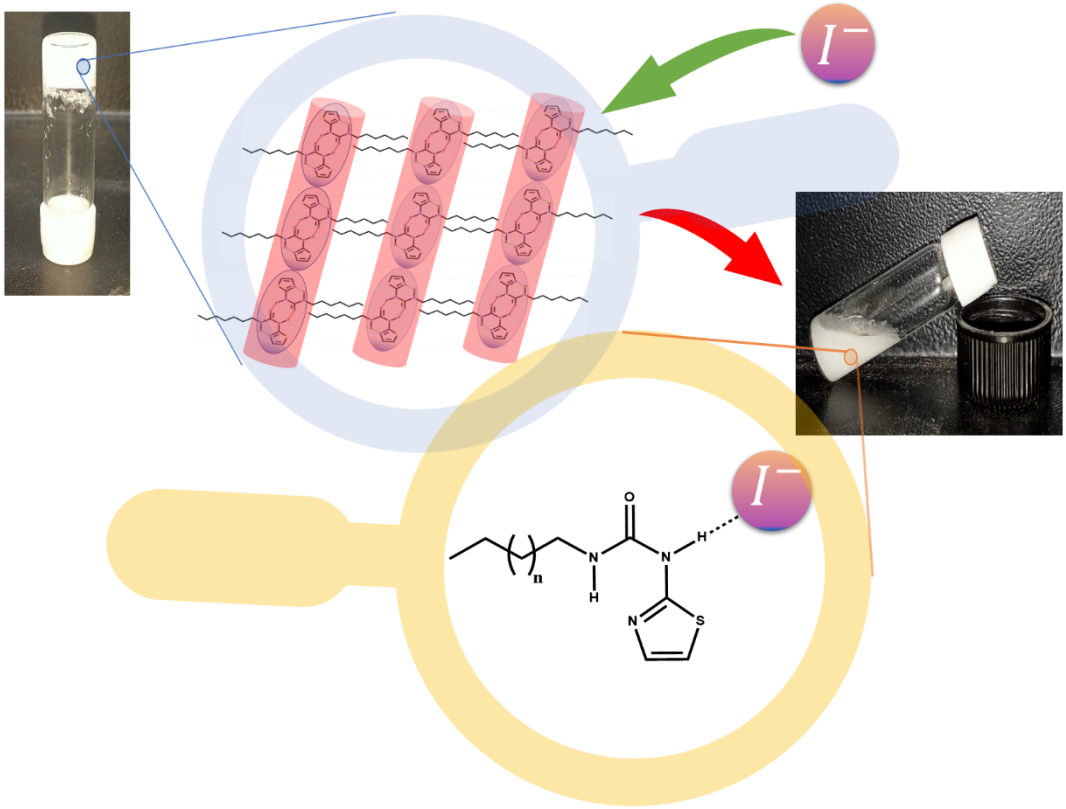

Scheme 3.6 *Probable mechanism of gelation and degelation after addition of powdered TBAI Salt.*

3.5 Conclusion

We have successfully demonstrated the simple strategy of designing molecules with components containing heterocyclic ring (thiazole moiety), 1-D hydrogen bonding sites (urea functional group), and a long aliphatic chain for inducing van der Waals interactions.

Seven newly synthesized compounds (**UTz 1–7**) displayed excellent gelation behaviour towards polar solvents and alcohol: water/ acetonitrile-water mixtures. SANS analysis of supramolecular assembly of compounds in solid-state suggested the formation of cylindrical assembly with a different molecular diameter strongly dependent upon the long aliphatic chain. The temperature variation SANS study on gel samples suggested a loose assembly of irregular fibers, which was further corroborated with SEM micrographs of xerogel. Interestingly, the iodide ion sensing ion in the solution and gel phase instead of chloride/fluoride ions (commonly sensed by urea-based compounds) prompted us to conclude the syn-anti conformation of the urea functional group, which was further supported by DFT calculation and NMR titration. The degelation (gel-to-sol) transition with the addition of iodide salts promises an attractive method of selective identification and detecting iodide ions. To the best of our knowledge, the LMOGs with iodide sensing are rarely reported in the literature and the present study provides an opportunity to design new LMOGs with potential applications such as iodide ion sensing.

References

1. Marangoni, A. G. & Garti, N. An Overview of the Past, Present, and Future of Organogels. in *Edible Oleogels: Structure and Health Implications* 1–17 (AOCS Press, 2011).
2. Richard G. Weiss, P. T. *Molecular Gels: Materials with Self-Assembled Fibrillar Networks*. *Molecular Gels* (Springer Dordrecht, 2006).
3. Yamanaka, M. Urea derivatives as low-molecular-weight gelators. *J. Incl. Phenom. Macrocycl. Chem.* **77**, 33–48 (2013).
4. Yadav, P. & Ballabh, A. Odd-even effect in a thiazole based organogelator: Understanding the interplay of non-covalent interactions on property and applications. *New J. Chem.* **39**, 721–730 (2015).
5. Yadav, P., Kour, D., Gupta, V. K., Rajnikant & Ballabh, A. Probing the role of weaker interactions in immobilization of solvents in a new class of supramolecular gelator. *RSC Adv.* **3**, 8417–8421 (2013).
6. Gronwald, O. & Shinkai, S. Sugar-Integrated Gelators of Organic Solvents. *Chem. - A Eur. J.* **7**, 4328–4334 (2001).
7. Sivakova, S. & Rowan, S. J. Nucleobases as supramolecular motifs. *Chem. Soc. Rev.* **34**, 9–21 (2005).
8. Žinić, M., Vögtle, F. & Fages, F. Cholesterol-based gelators. *Top. Curr. Chem.* **256**, 39–76 (2005).
9. Dastidar, P. Supramolecular gelling agents : can they be designed ? *Chem. Soc. Rev.Rev.* **37**, 2699–2715 (2008).
10. Bhardwaj, V. & Ballabh, A. A series of multifunctional pivalamide based Low Molecular Mass Gelators (LMOGs) with potential applications in oil-spill remediation and toxic dye removal. *Colloids Surfaces A Physicochem. Eng. Asp.* **632**, 127813 (2021).
11. Kapuścińska, A. & Nowak, I. The use of urea and its derivatives in the cosmetics industry. *Chemik* **68**, 91–96 (2014).
12. Steed, J. W. Anion-tuned supramolecular gels: A natural evolution from urea supramolecular chemistry. *Chem. Soc. Rev.* **39**, 3686–3699 (2010).
13. Wang, A. Y., Lu, Y., Zhu, H. L. & Jiao, Q. C. A urea derivative with marked antitumor activities. *Oncol. Lett.* **3**, 373–376 (2012).
14. Abdelazeem, A. H., Habash, M., Maghrabi, I. A. & Taha, M. O. Synthesis and evaluation of novel diphenylthiazole derivatives as potential anti-inflammatory agents. *Med. Chem. Res.* **24**, 3681–3695 (2015).
15. Biswakarma, D., Dey, N. & Bhattacharya, S. A biocompatible hydrogel as a template for oxidative decomposition reactions: A chemodosimetric analysis and in vitro imaging of hypochlorite. *Chem. Sci.* **13**, 2286–2295 (2022).
16. Bhaskara Reddy, M. V., Srinivasulu, D., Peddanna, K., Apparao, C. & Ramesh, P. Synthesis and Antioxidant Activity of New Thiazole Analogues Possessing Urea, Thiourea, and Selenourea Functionality. *Synth. Commun.* **45**, 2592–2600 (2015).
17. Dayan, F. E. *et al.* Amino- and urea-substituted thiazoles inhibit photosynthetic electron transfer. *J. Agric. Food Chem.* **48**, 3689–3693 (2000).
18. Sroor, F. M., Abdelmoniem, A. M. & Abdelhamid, I. A. Facile Synthesis, Structural Activity Relationship, Molecular Modeling and In Vitro Biological Evaluation of New Urea Derivatives with Incorporated Isoxazole and Thiazole Moieties as Anticancer Agents. *ChemistrySelect* **4**, 10113–10121 (2019).
19. Verheesen, R. H. & Schweitzer, C. M. Iodine deficiency, more than cretinism

and goiter. *Med. Hypotheses* **71**, 645–648 (2008).
20. Pienpinijtham, P., Han, X. X., Ekgasit, S. & Ozaki, Y. Highly sensitive and selective determination of iodide and thiocyanate concentrations using surface-enhanced Raman scattering of starch-reduced gold nanoparticles. *Anal. Chem.* **83**, 3655–3662 (2011).
21. Bakker, E., Pretsch, E. & Bühlmann, P. Selectivity of potentiometric ion sensors. *Anal. Chem.* **72**, 1127–1133 (2000).
22. Li, Y. J., Tseng, Y. T., Unnikrishnan, B. & Huang, C. C. Gold-nanoparticles-modified cellulose membrane coupled with laser desorption/ionization mass spectrometry for detection of iodide in urine. *ACS Appl. Mater. Interfaces* **5**, 9161–9166 (2013).
23. Aswal, V. K. & Goyal, P. S. Small-angle neutron scattering diffractometer at Dhruva reactor. *Curr. Sci.* **79**, 947–953 (2000).
24. Takata, S. I., Norisuye, T. & Shibayama, M. Small-angle neutron-scattering study on preparation temperature dependence of thermosensitive gels. *Macromolecules* **35**, 4779–4784 (2002).
25. Shibayama, M. Small-angle neutron scattering on polymer gels: Phase behavior, inhomogeneities and deformation mechanisms. *Polym. J.* **43**, 18–34 (2011).
26. Saffer, E. M. *et al.* SANS study of highly resilient poly(ethylene glycol) hydrogels. *Soft Matter* **10**, 1905 (2014).
27. Chen, S. H. & Teixeira, J. Structure and fractal dimension of protein-detergent complexes. *Phys. Rev. Lett.* **57**, 2583–2586 (1986).
28. Teixeira, J. Small-angle scattering by fractal systems. *J. Appl. Crystallogr.* **21**, 781–785 (1988).
29. Pal, A. & Dey, J. Water-Induced Physical Gelation of Organic Solvents by N -(n -Alkylcarbamoyl)-L-alanine Amphiphiles. *Langmuir* **27**, 3401–3408 (2011).
30. Suzuki, M., Nakajima, Y., Yumoto, M., Kimura, M. & Hanabusa, K. In situ organogelation at room temperature : direct synthesis of gelators in organic solvents. *Org. Biomol. Chem.* **2**, 1155–1159 (2004).
31. Avramiotis, S. *et al.* Lecithin Organogels Used as Bioactive Compounds Carriers . A Microdomain Properties Investigation. *Langmuir* **23**, 4438–4447 (2007).
32. Zweep, N. *et al.* Balancing hydrogen bonding and van der waals interactions in cyclohexane-based bisamide and bisurea organogelators. *Langmuir* **25**, 8802–8809 (2009).
33. Mido, Y. An infrared study of various dialkylureas in solution. *Spectrochim. Acta Part A* **29A**, 431–438 (1973).
34. Piasek Z. & Urbanski T. The Infrared Absorption Spectrum and Structure of Urea. *Bul. L' Acad. Pol. Des Sci.* **X**, 113–120 (1962).
35. Higashi, A., Czarnecki, M. A. & Ozaki, Y. Infrared study of solids and cast films of long-chain fatty acids. *Thin Solid Films* **230**, 203–208 (1993).
36. Das, D., Kar, T. & Das, P. K. Gel-nanocomposites: Materials with promising applications. *Soft Matter* **8**, 2348–2365 (2012).
37. Shen, J. S., Mao, G. J., Zhou, Y. H., Jiang, Y. B. & Zhang, H. W. A ligand-chirality controlled supramolecular hydrogel. *Dalt. Trans.* **39**, 7054–7058 (2010).
38. Yu, G., Yan, X., Han, C. & Huang, F. Characterization of supramolecular gels. *Chem. Soc. Rev.* **42**, 6697–6722 (2013).
39. Proeerjliw, E., Anthraquinone--carboxylate, C., Ostuni, E., Kamaras, P. &

Weiss, R. G. Novel X-ray Method for In Situ Determination of Gelator Strand Structure: Polymorphism of Cholesteryl. *Angew. Chem. Int. Ed.* **35**, 1324–1326 (1996).

40. Patel, A. M., Ray, D., Aswal, V. K. & Ballabh, A. Probing the mechanism of gelation and anion sensing capability of a thiazole based amide gelator: A case study. *Colloids Surfaces A Physicochem. Eng. Asp.* **607**, 125430 (2020).
41. baddi, S., Sarma, D. S. & Palanisamy, A. Self-assembly of aromatic biscarbamate gelators: effect of spacer length on the gelation and rheology. *J. Sol-Gel Sci. Technol.* **79**, 637–649 (2016).
42. Phukan, N. & Baruah, J. B. Conformational adjustments over synthons of urea and thiourea based assemblies. *CrystEngComm* **18**, 7753–7763 (2016).
43. Cox, C. & Lectka, T. Solvent Effects on the Barrier to Rotation in Carbamates Table 1. Solvent Effects on the Barrier to Rotation of Amide 1 and Carbamate 2 a. *J. Org. Chem.* **63**, 2426–2427 (1998).
44. Rablen, P. R. *et al.* Solvent Effects on the Barrier to C−N Bond Rotation in N,N-Dimethylaminoacrylonitrile: Modeling by Reaction Field Theory and by Monte Carlo Simulations. *J. AM. CHEM. SOC* **121**, 218–226 (1999).
45. Smith, A. E. The crystal structure of the urea–hydrocarbon complexes. *Acta Crystallogr.* **5**, 224–235 (1952).
46. Harris, K. D. M. & Thomas, J. M. Structural aspects of urea inclusion compounds and their investigation by X-ray diffraction: A general discussion. *J. Chem. Soc. Faraday Trans.* **86**, 2985–2996 (1990).
47. Robert G. Parr, W. Y. Density-Functional Theory of the Electronic. *Annu. Rev. Phys. Chem.* **46**, 701–728 (1995).
48. Phukan, N. & Baruah, J. B. Polymorphs of 1-(5-methylthiazol-2-yl)-3-phenylthiourea and various anion-assisted assemblies of two positional isomers. *Cryst. Growth Des.* **14**, 2640–2653 (2014).
49. Rohan A. Hule†, Radhika P. Nagarkar‡, Boualem Hammouda§, Joel P. Schneider‡, and D. J. P. Dependence of Self-Assembled Peptide Hydrogel Network Structure on Local Fibril Nanostructure. *Macromolecules* **42**, 7137–7145 (2009).
50. Mears, L. L. E. *et al.* Drying Affects the Fiber Network in Low Molecular Weight Hydrogels. *Biomacromolecules* **18**, 3531–3540 (2017).
51. Shibayama, M. Structure-mechanical property relationship of tough hydrogels. *Soft Matter* **8**, 8030–8038 (2012).
52. Yang, Z. *et al.* Nonlinear Behavior of Gelatin Networks Reveals a Hierarchical Structure. *Biomacromolecules* **17**, 590–600 (2016).
53. Yang, X., Zhang, G. & Zhang, D. Stimuli responsive gels based on low molecular weight gelators. *J. Mater. Chem.* **22**, 38–50 (2012).
54. Park, S., Ju, J., Lee, Y. J. & Lee, S. Y. A hydrazide organogelator for fluoride sensing with hyperchromicity and gel-to-sol transition. *RSC Adv.* **10**, 14243–14248 (2020).
55. Rajamalli, P. & Prasad, E. Low molecular weight fluorescent organogel for fluoride ion detection. *Org. Lett.* **13**, 3714–3717 (2011).
56. Piepenbrock, M. M., Lloyd, G. O., Clarke, N. & Steed, J. W. Metal- and Anion-Binding Supramolecular Gels. *Chem. Rev.* **110**, 1960–2004 (2010).
57. Biswakarma, D., Dey, N. & Bhattacharya, S. A thermo-responsive supramolecular hydrogel that senses cholera toxin: Via color-changing response. *Chem. Commun.* **56**, 7789–7792 (2020).
58. Samanta, S. K., Dey, N., Kumari, N., Biswakarma, D. & Bhattacharya, S.

Multimodal Ion Sensing by Structurally Simple Pyridine-End Oligo p-Phenylenevinylenes for Sustainable Detection of Toxic Industrial Waste. *ACS Sustain. Chem. Eng.* **7**, 12304–12314 (2019).

59. Maiti, B., Bhattacharjee, S. & Bhattacharya, S. Perfluoroarene induces a pentapeptidic hydrotrope into a pH-tolerant hydrogel allowing naked eye sensing of Ca 2+ ions. *Nanoscale* **11**, 2223–2230 (2019).
60. Bhattacharjee, S. & Bhattacharya, S. Pyridylenevinylene based Cu2+-specific, injectable metallo(hydro)gel: Thixotropy and nanoscale metal-organic particles. *Chem. Commun.* **50**, 11690–11693 (2014).
61. Panja, S. & Adams, D. J. Stimuli responsive dynamic transformations in supramolecular gels. *Chem. Soc. Rev.* **50**, 5165–5200 (2021).
62. Jayabhavan, S. S., Ghosh, D. & Damodaran, K. K. Making and breaking of gels: Stimuli-responsive properties of bis(pyridyl-n-oxide urea) gelators. *Molecules* **26**, (2021).
63. Bhattacharya, S. & Thomas, M. Synthesis of a novel thiazole based dipeptide chemosensor for Cu(II) in water. *Tetrahedron Lett.* **41**, 10313–10317 (2000).
64. Blažek Bregović, V., Basarić, N. & Mlinarić-Majerski, K. Anion binding with urea and thiourea derivatives. *Coord. Chem. Rev.* **295**, 80–124 (2015).
65. Amendola, V., Esteban-Gómez, D., Fabbrizzi, L. & Licchelli, M. What anions do to N-H-containing receptors. *Acc. Chem. Res.* **39**, 343–353 (2006).
66. Ghosh, K., Panja, S. & Bhattacharya, S. Naphthalene linked pyridyl urea as a supramolecular gelator: a new insight into naked eye detection of I- in the gel state with semiconducting behaviour. *RSC Adv.* **5**, 72772–72779 (2015).
67. Shen, J. S., Li, D. H., Cai, Q. G. & Jiang, Y. B. Highly selective iodide-responsive gel-sol state transition in supramolecular hydrogels. *J. Mater. Chem.* **19**, 6219–6224 (2009).
68. Wygladacz, K. & Bakker, E. Fluorescent microsphere fiber optic microsensor array for direct iodide detection at low picomolar concentrations. *Analyst* **132**, 268–272 (2007).

Supplementary data

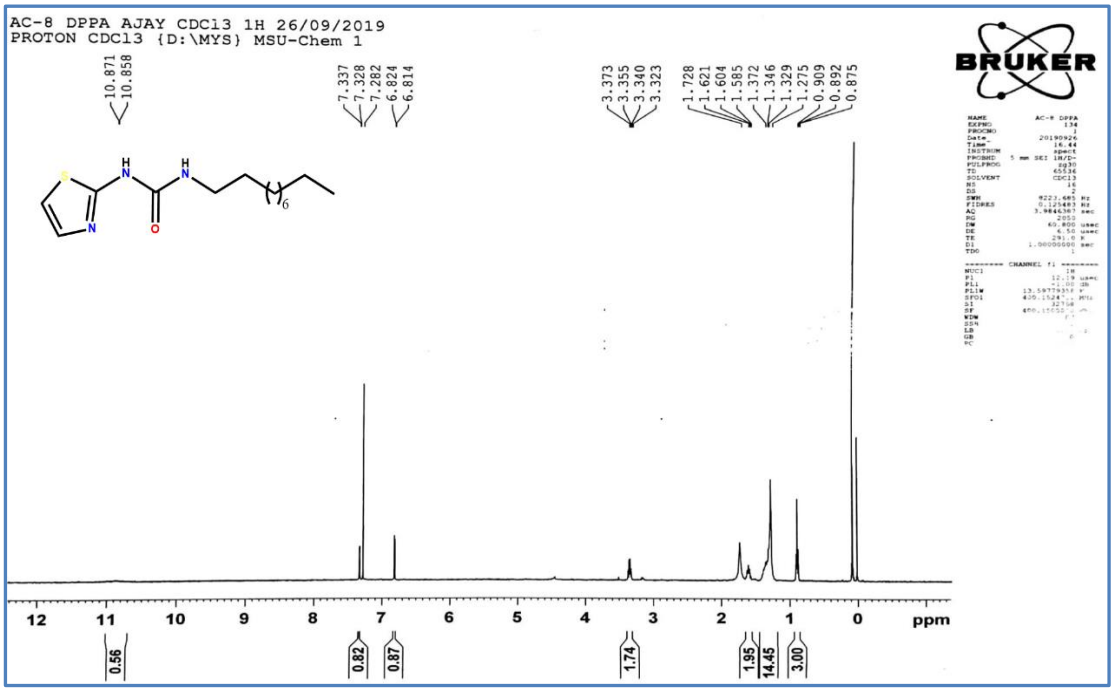

Figure 33 *NMR spectra of UTz-1*

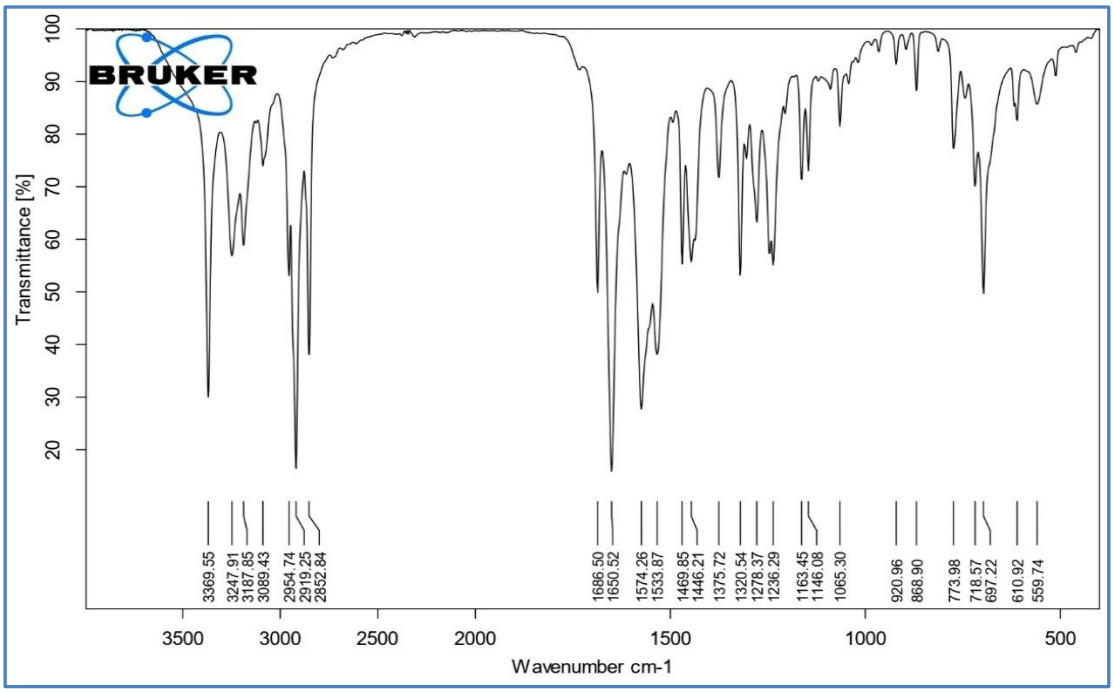

Figure 34 *IR Spectra of UTz -1*

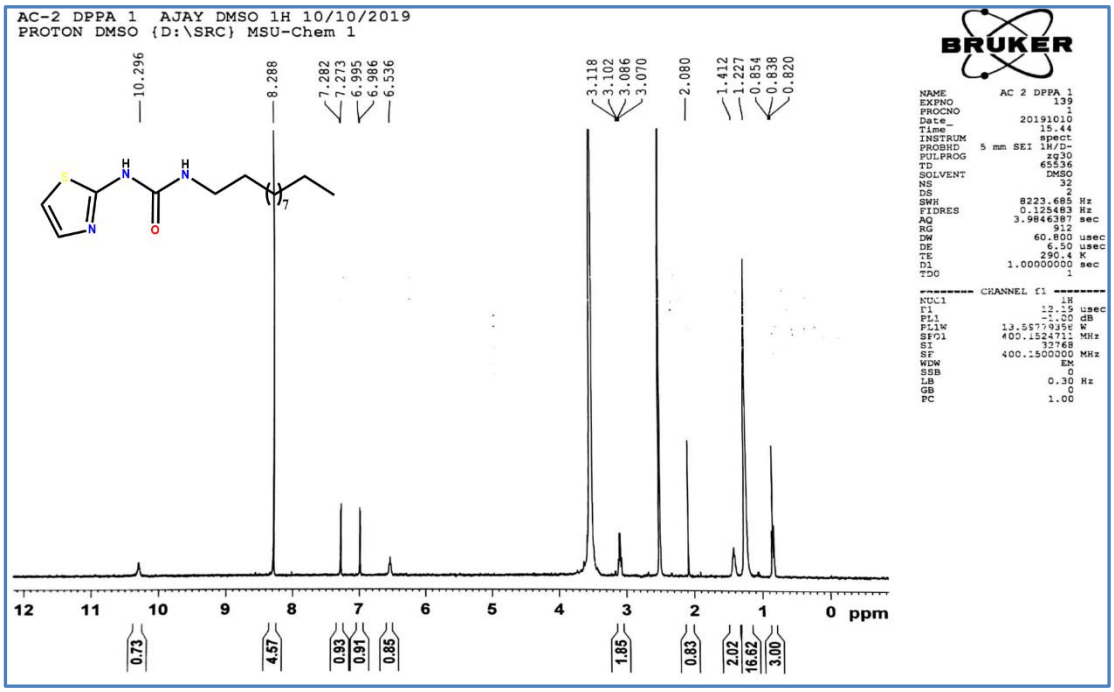

Figure 35 *NMR spectra of UTz-2*

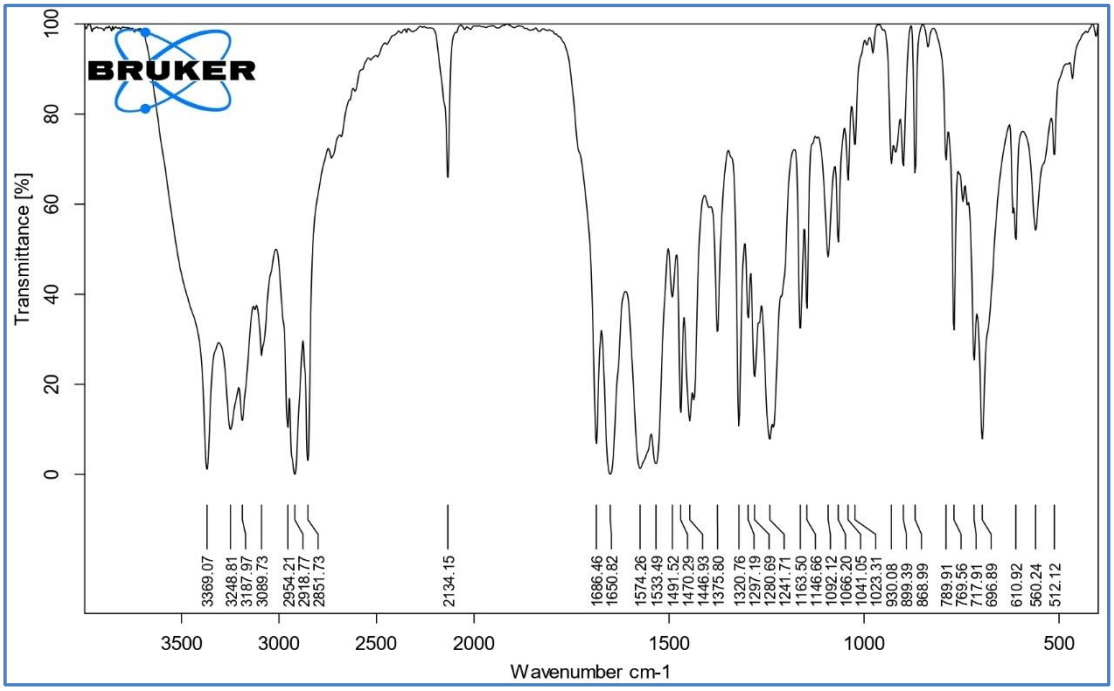

Figure 36 *IR Spectra of UTz-2*

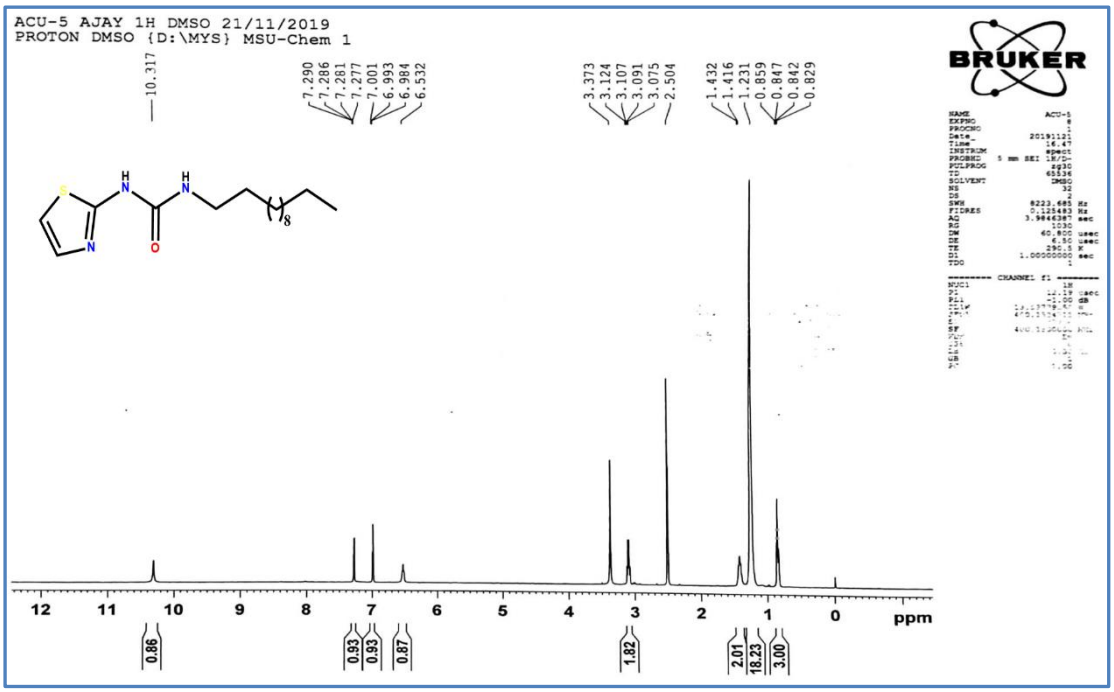

Figure 37: *NMR spectra of UTz-3*

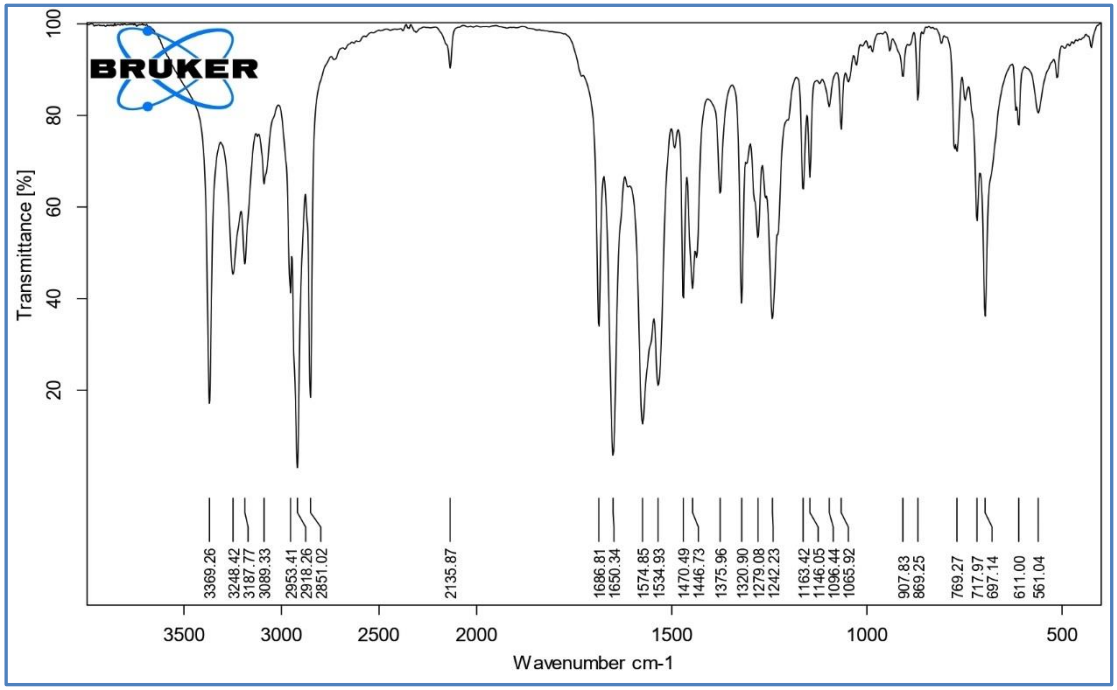

Figure 38: *IR Spectra of UTz-3*

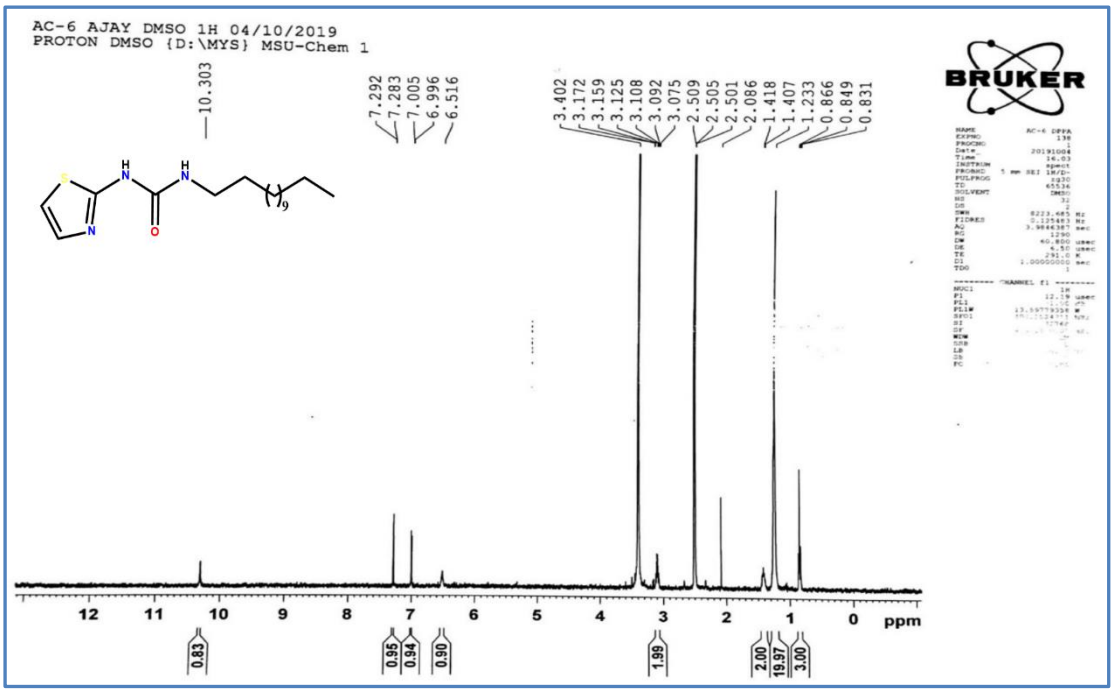

Figure 39 *NMR spectra of UTz-4*

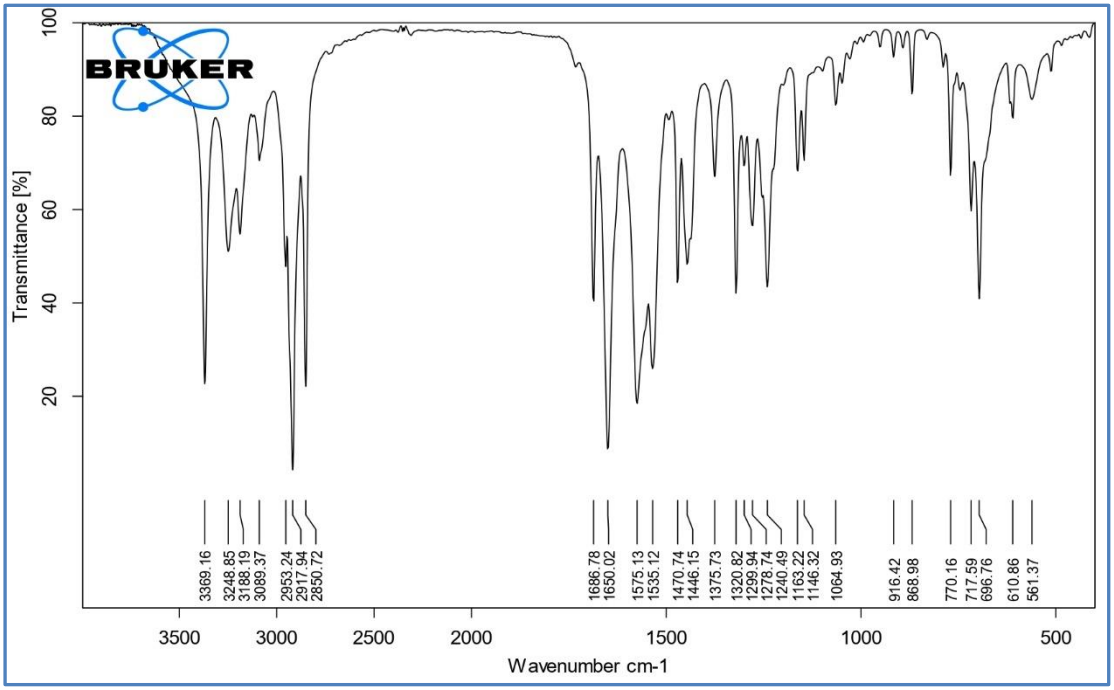

Figure 40 *IR Spectra of UTz-4*

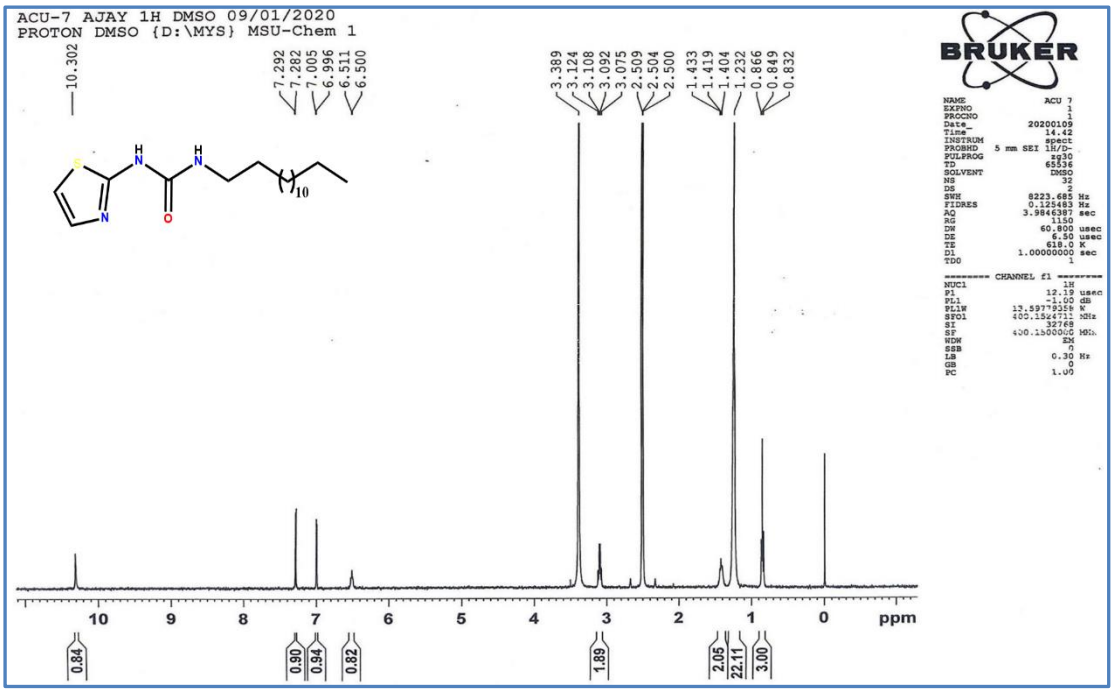

Figure 41 *NMR spectra of UTz-5*

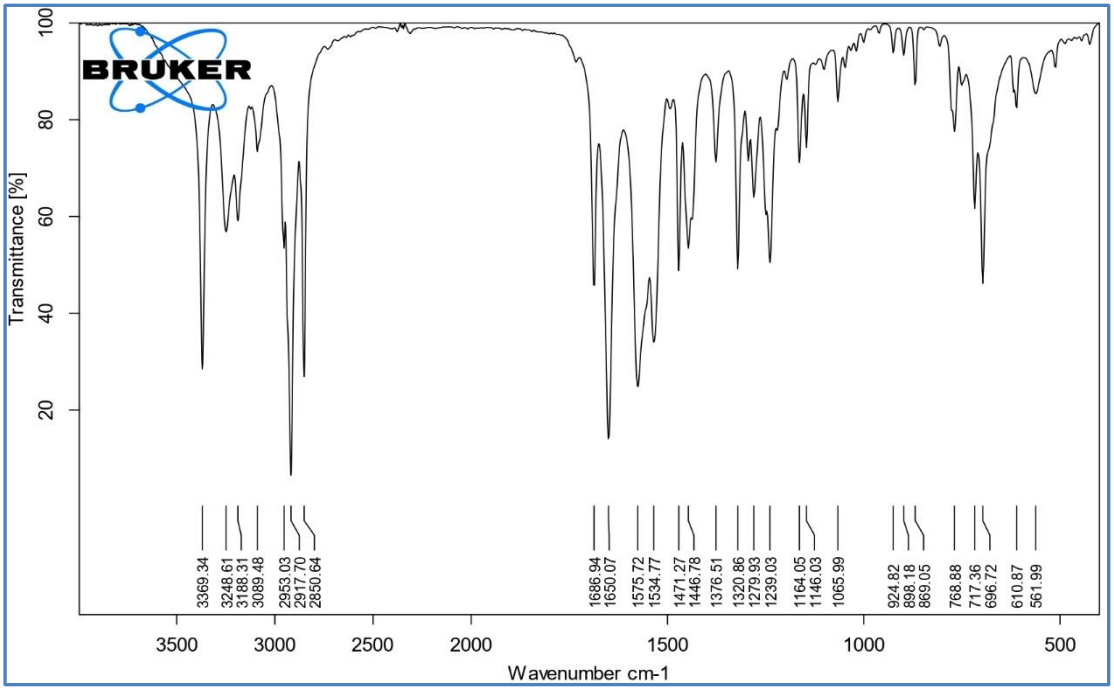

Figure 42 *IR Spectra of UTz-5*

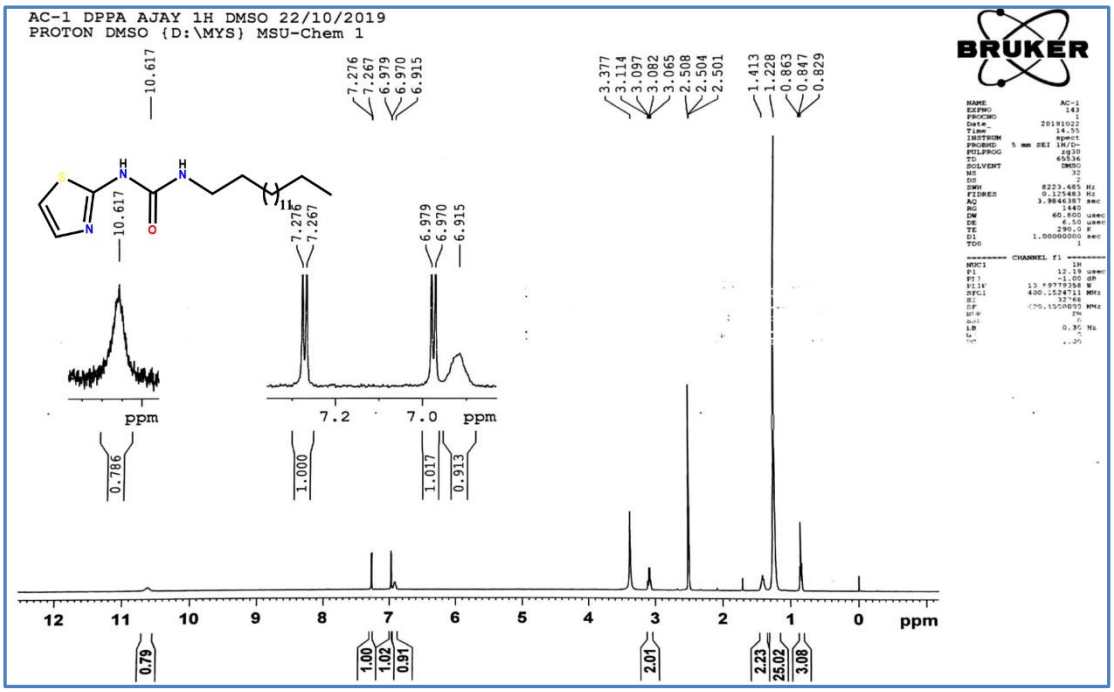

Figure 43 *NMR spectra of UTz-6*

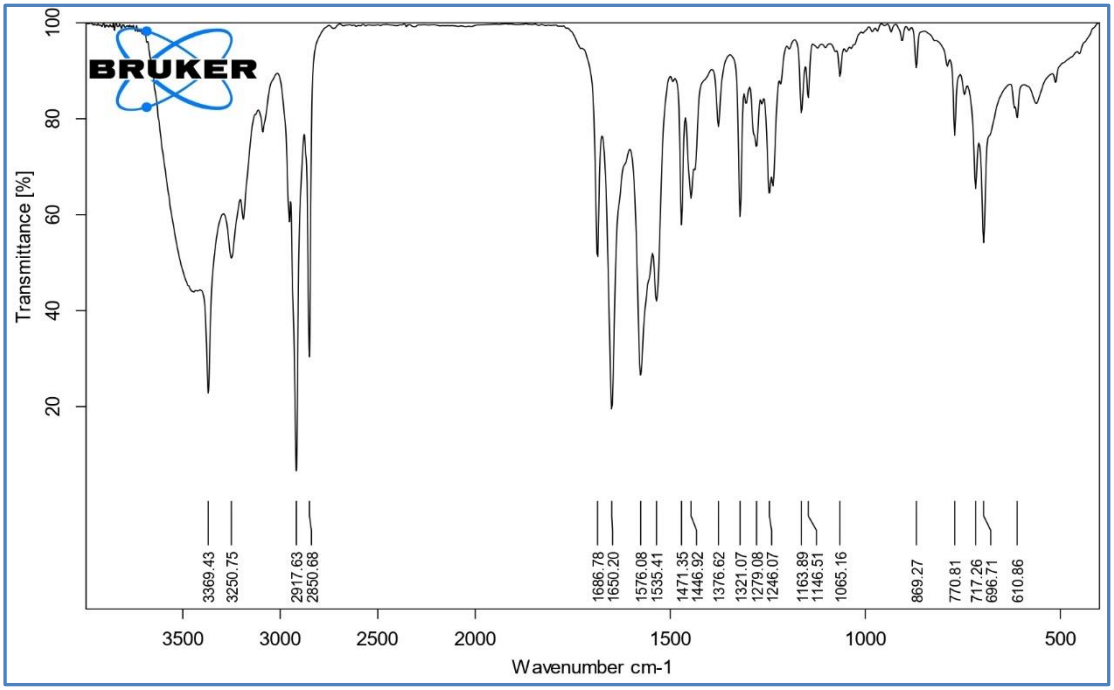

Figure 44 *IR Spectra of UTz-6*

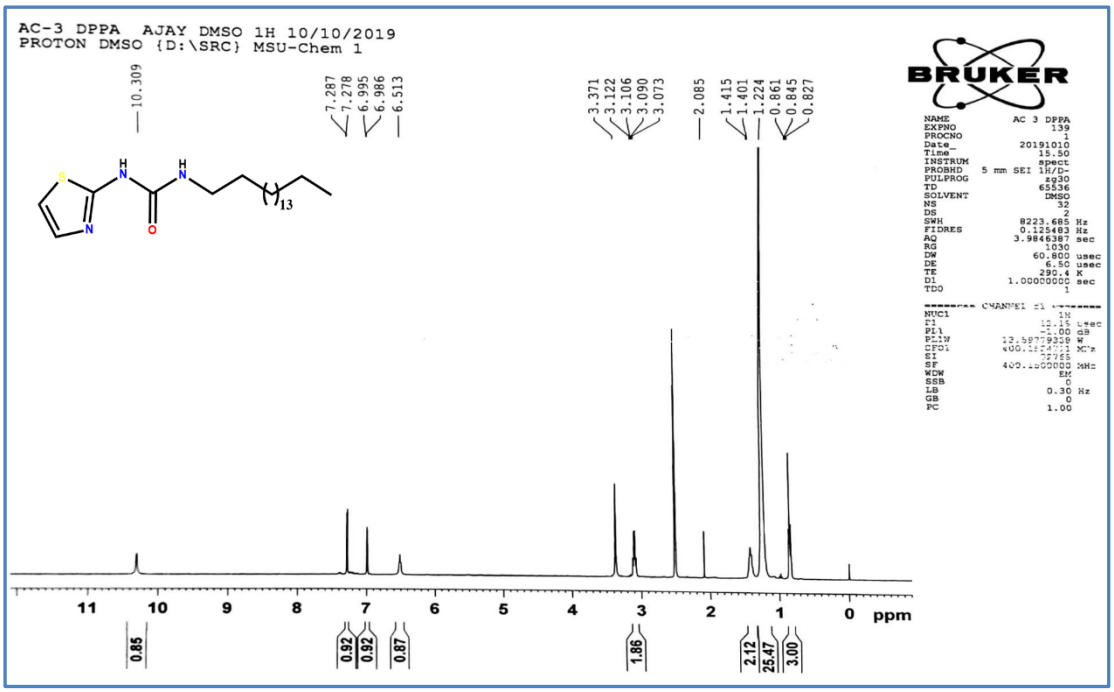

Figure 45 *NMR spectra of UTz-7*

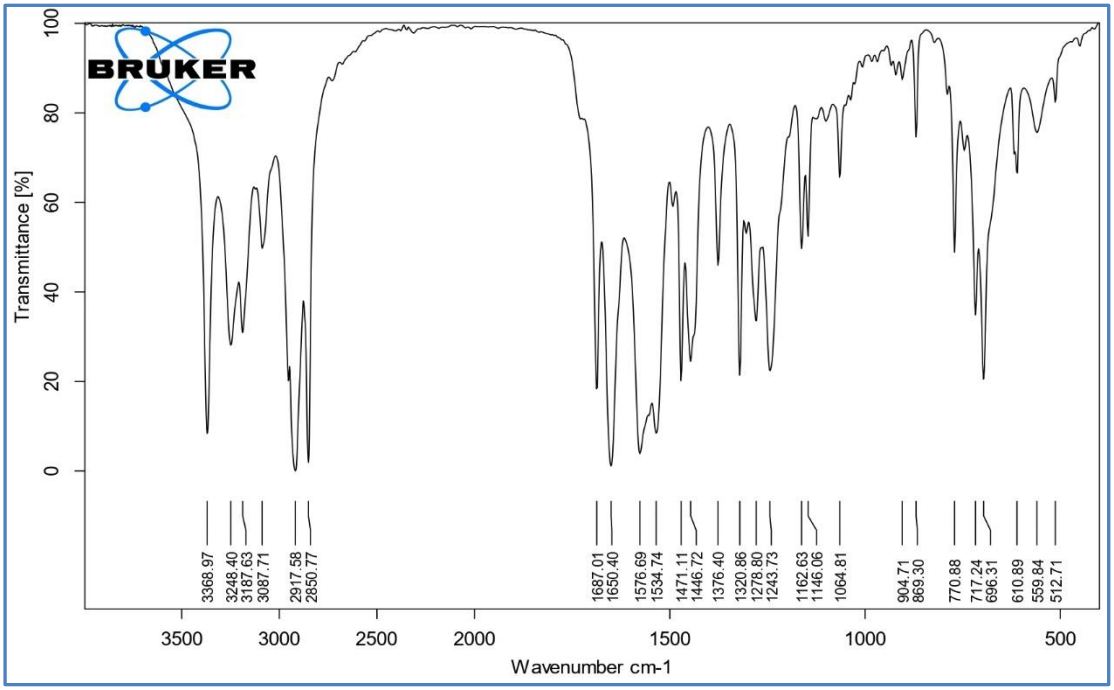

Figure 46 *IR Spectra of UTz-7*